Evidence of haze-driven secondary production of supermicrometer aerosol nitrate and sulfate in size distribution data in South Korea

Joseph S. Schlosser[1], Connor Stahl[1], Armin Sorooshian[1,2], Yen Thi-Hoang Le[3], Ki-Joon Jeon[3,4,5], Peng Xian[6], Carolyn E. Jordan[7,8], Katherine R. Travis[7], James H. Crawford[7], Sung Yong Gong[9], Hye-Jung Shin[10], In-Ho Song[10], Jong-sang Youn[5,11]

[1]Department of Chemical and Environmental Engineering, University of Arizona, Tucson, Arizona, USA
[2]Department of Hydrology and Atmospheric Sciences, University of Arizona, Tucson, Arizona, USA
[3]Program in Environmental and Polymer Engineering, Inha University, 100 Inha-ro, Incheon 22212, Republic of Korea.
[4]Department of Environmental Engineering, Inha University, 100 Inha-ro, Incheon 22212, Republic of Korea.
[5]Particle Pollution Research and Management Center, Incheon 21999, Republic of Korea
[6]Marine Meteorology Division, Naval Research Laboratory, Monterey, CA, USA
[7]NASA Langley Research Center, Hampton, VA, USA
[8]National Institute of Aerospace, Hampton, VA, USA
[9]Climate, Air Quality and Safety Research Group/Division for Atmospheric Environment, Korea Environment Institute, 370 Sicheong-daero, Sejong 30147, Republic of Korea
[10]Air Quality Research Division, Climate and Air Quality Research Department, National Institute of Environmental Research, 42 Hwangyoun-ro, Incheon 22689, Republic of Korea
[11]Department of Energy and Environmental Engineering, the Catholic University of Korea, 43 Jibong-ro, Bucheon 14662, Republic of Korea

Correspondence to: Jong-sang Youn (jsyoun@catholic.ac.kr) and Armin Sorooshian (armin@arizona.edu)

Abstract. This study reports measurements of size-resolved aerosol composition at a site in Incheon along with other aerosol characteristics for contrast between Incheon (coastal) and Seoul (inland), South Korea, during a transboundary pollution event during the early part of an intensive sampling period between 4 and 11 March 2019. Anthropogenic emissions were dominant in the boundary layer over the study region between 4 and 6 March, with much smaller contributions from dust, smoke, and sea salt. The meteorology of this period (shallow boundary layer, enhanced humidity, and low temperature) promoted local heterogeneous formation of secondary inorganic and organic species, including high nitrate (NO_3^-) relative to sulfate (SO_4^{2-}). Seoul exhibited higher $PM_{2.5}$ levels than Incheon likely due to local emissions. The following findings point to secondary aerosol formation and growth sensitivity to water vapor during this pollution event: (i) significant concentrations of individual inorganic and organic acids in the supermicrometer range relative to their full size range (~40%) at higher humidity; (ii) high correlation ($r = 0.95$) between oxalate and SO_4^{2-}, a marker of secondary aqueous production of oxalate; (iii) increased sulfur and nitrogen oxidation ratios as a function of humidity; and (iv) matching composition apportionment (for soluble ions) between the PM_1 and $PM_{2.5-1}$ size fractions. The last finding confirms that PM_1 aerosol composition measurements fully capture $PM_{2.5}$ composition apportionment (for soluble ions) during haze events and, therefore, may be reliably applied in modeling studies of such events over the full $PM_{2.5}$ size range. The study period was marked by relatively low temperatures that made NO_3^- the most abundant species detected, pointing to the sensitivity of $PM_{2.5}$ levels and composition as a function of season during such transboundary events. For instance, other such events in previous studies exhibited more comparable levels between SO_4^{2-} and NO_3^- coincident with higher temperatures than the current study. This dataset can contribute to future evaluation of model $PM_{2.5}$ composition to better support regulatory efforts to control $PM_{2.5}$ precursors.

1 Introduction

South Korea has been the focus of extensive air quality research in recent years owing to continuing challenges as it is a growing metropolitan center with extensive sources of pollution both locally and regionally (Lee and Kim, 2007;Guttikunda et al., 2003). Although direct emission control policies have reduced primary pollutant concentrations over time (e.g., lead, carbon monoxide, sulfur dioxide), there has been less success to reduce levels of secondarily formed pollutants associated with particulate matter with diameters (D) less than or equal to 2.5 μm ($PM_{2.5}$) (Kim and Lee, 2018). A common phenomenon leading to significant aerosol concentrations over large parts of South Korea is transboundary pollution events stemming from areas such as China (Choi et al., 2019b;Choi et al., 2019a;Peterson et al., 2019;Lee et al., 2019b;Eck et al., 2020;Cha et al., 2019) that impact both coastal and inland parts of the peninsula. These events include dust (Heim et al., 2020;Kim et al., 2012), industrial and agricultural burning emissions (Lamb et al., 2018), sea salt (Lee et al., 2018), and wildfire plumes from Siberia (Lamb et al., 2018) that are superimposed on the local pollution sources that include biogenic emissions, urban and vehicular emissions, shipping emissions, industrial activities, and biomass burning (Park et al., 2021;Lamb et al., 2018).

While the influence of long-range transport on the Korean peninsula's air quality has been demonstrated (Lee et al., 2021;Koo et al., 2018), a question remains about the relative contributions of transboundary versus local emissions. Results from the Megacity Air Pollution Studies-Seoul (MAP-Seoul) study (May – June 2015) indicated that advected pollution from China mostly affects western coastal sites and that local emissions are significant in accounting for Seoul's radiation-absorbing aerosol particles (Lee et al., 2018). Others have pointed to the importance of domestic emissions during transboundary pollution events, especially when transport rates are below ~250 km day^{-1} (Lee et al., 2019b). Studies from the Korea-United States Air Quality (KORUS-AQ) campaign (1 May – 10 June 2016) showed that during transboundary pollution episodes, Seoul (inland) exhibited significantly higher levels of $PM_{2.5}$ than coastal areas (Eck et al., 2020). Nault et al. (2018) showed with in-situ measurements that local emissions are the primary contributor to secondary organic aerosol (SOA) over Seoul. Furthermore, diurnal variations in aerosol optical depth (AOD) are also more significant at inland sites versus coastal sites (Lennartson et al., 2018). In their analysis of the same pollution episode as our study in early March 2019, Lee et al. (2019a) showed that the foreign contribution to $PM_{2.5}$ in Seoul was 78.8% as compared to 21.2% from domestic sources based on the Community Multiscale Air Quality (CMAQ) model. It is important to note that such apportionments are sensitive to the modeled composition of $PM_{2.5}$ as discussed in Choi et al. (2019a) and Jordan et al. (2020). Hence, comparisons of measured and modeled $PM_{2.5}$ composition are needed to validate apportionment between domestic and transported pollutants.

Local and upwind meteorology have been shown to play a major role in modulating temporal trends in PM and gas pollutant levels over South Korea (Seo et al., 2018;Cho et al., 2021;Jordan et al., 2020;Koo et al., 2020;Peterson et al., 2019;Ryu et al., 2021). Models have yet to adequately capture sulfate (SO_4^{2-}) formation in East Asian haze events (Shao et al., 2019) as they generally underestimate SO_4^{2-} in haze, while the KORUS-AQ study also revealed that nitrate (NO_3^-) formation in haze may be simultaneously overestimated resulting in errors in aerosol liquid water content and other modeled properties (Jordan et al., 2020). Other recent studies of East Asian haze have pointed to the importance of secondary aerosol formation, primarily ammonium sulfate and nitrate salts, with additional SOA (Hu et al., 2014;Huang et al., 2014;Cheng et al., 2016;Li et al., 2018;Zhang et al., 2017). Moisture and thus aerosol-laden water have been shown to be especially important to promote the formation of these secondary species (Wu et al., 2018;Zhang et al., 2018;Wang et al., 2016;Zhang et al., 2017). The May-June 2016 period of KORUS-AQ offered a detailed view of frontal passages transporting pollution from China to the Korean peninsula under cloudy and humid conditions that promoted haze and fog formation within a shallow stable boundary layer (Jordan et al., 2020;Peterson et al., 2019). Sulfate and NO_3^- formation was observed to be efficient owing to heterogeneous processing with the former fueled by local and transported sulfur dioxide (SO_2) and the latter from local nitrogen oxides (NO_x) and enhanced nocturnal NO_3 radical reactions. A positive feedback was suggested whereby increased water uptake by particles increased gas-to-particle partitioning, which in turn further increased water uptake. Furthermore, clouds reduced transmission of solar radiation to the surface, thereby reducing mixing and leading to more PM accumulation in a shallow boundary layer. Jordan et al. (2020) called for more detailed aerosol and meteorological measurements co-located with AirKorea sites (https://www.airkorea.or.kr/eng) that routinely monitor $PM_{2.5}$ and other basic pollutants (PM_{10}, O_3, SO_2, NO_2, CO) in order to advance knowledge of aerosol lifecycle behavior over the Korean peninsula.

Aerosol composition provides important evidence for impacts of meteorology and atmospheric circulation on PM, which are sometimes challenging to reproduce in models. The current study exploits an Incheon dataset of size-resolved composition during a major pollution episode in March 2019 to expand on the evidence for these impacts and to help interpret observations from the larger network of ongoing Korean observations. Data were collected at both Incheon near the western coast of South Korea and at the inland city of

Seoul (Fig. 1), which allows for a critical look at how $PM_{2.5}$ levels compare between the sites and if Seoul has higher levels (suggesting local $PM_{2.5}$ production) as described by Eck et al. (2020) and Jordan et al. (2020). This study examines the role for meteorological parameters like humidity in impacting size-resolved aerosol composition. This is especially important since past studies have mainly focused on bulk PM_1, $PM_{2.5}$ or PM_{10} (Park et al., 2018;Ryu and Min, 2021;Seo et al., 2018;Won et al., 2020). Size-resolved composition data are pertinent to improve understanding of how particles in the region impact cloud formation, visibility, and public health, all of which are sensitive to size-specific aerosol properties.
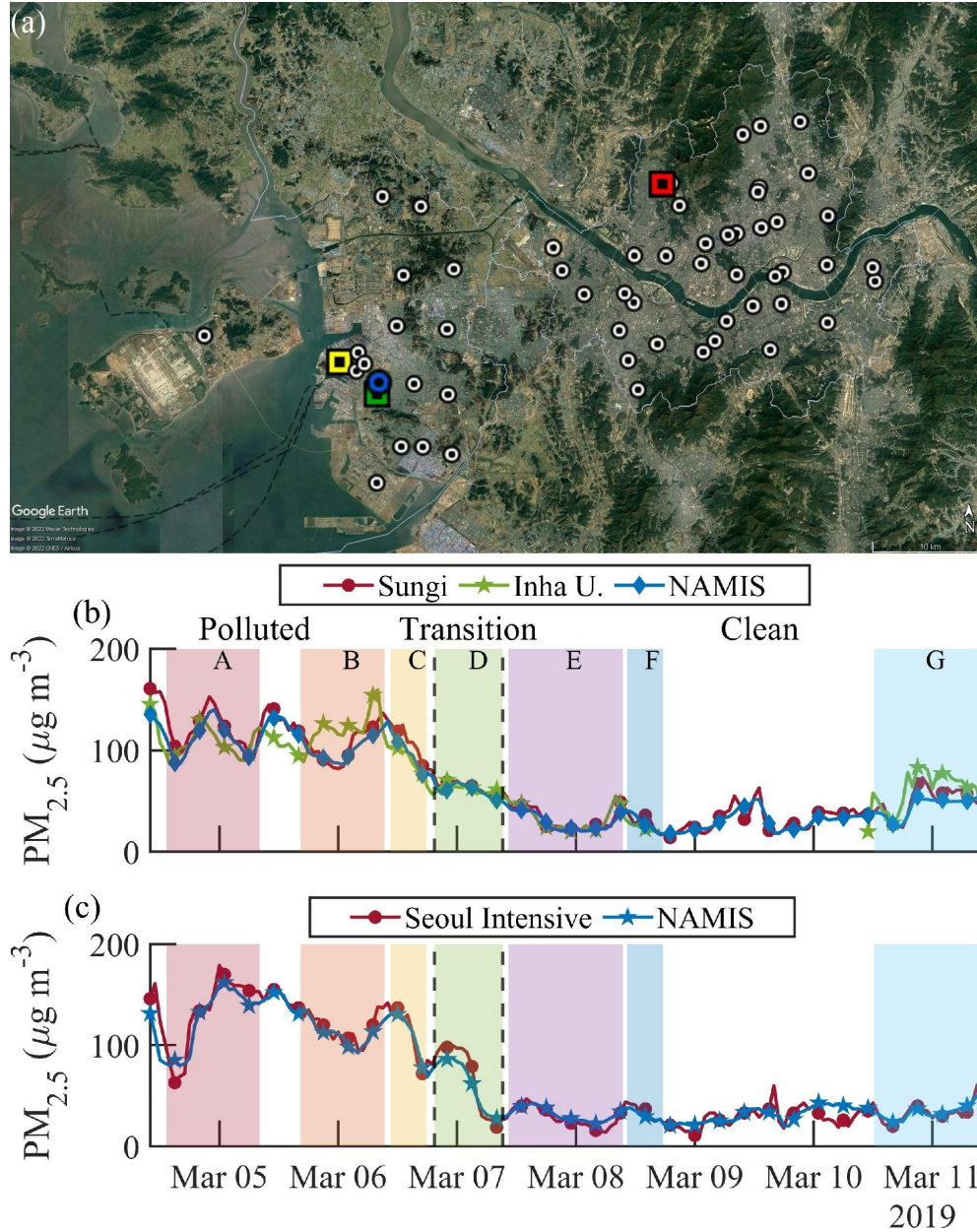
Figure 1. (a) Spatial map showing the 17 and 40 National Ambient air quality Monitoring Information System (NAMIS) stations in Incheon and Seoul, respectively, along with the three main surface sites relied on for this study (yellow = Incheon meteorological site, green = Inha University, blue = Sungi [also a NAMIS station], red = Seoul Intensive Monitoring Station). $PM_{2.5}$ comparison between (b) city-wide Incheon mean values and those for Sungi and Inha University, and between (c) city-wide Seoul mean values and those for Seoul Intensive Monitoring Station. Coefficients of determination (R^2) between the data points: (b) (Inha University) $R^2 = 0.82$ and (Sungi) $R^2 = 0.98$; (c) $R^2 = 0.96$. Shaded regions of panels

b-c are labeled with individual DLPI+ sets overlapping in time. All times are reported in Korea standard time (KST), where KST is UTC + 9 hrs.

2 Datasets and Methods

During the period between 4 and 11 March 2019, there was a major regional haze pollution event that impacted Incheon and Seoul monitoring sites. The haze event lasted for approximately the first three days and then the air quality improved between 7 and 11 March (Figs. 1-2). We consider the period from 4 March 10:00 – 6 March 19:00 as "polluted", from 6 March 19:00 – 7 March 09:15 as "transition", and 7 March 09:15 – 11 March 10:00 as "clean"; these time definitions are chosen based on start/stop times of size-resolved impactor measurements conducted in Incheon (Sect. 2.1.1) during periods with higher, intermediate, and lower PM concentrations (e.g., Figs. 1-2). Times in this study are in Korea standard time (KST), where KST = UTC + 9 hours. This study relies on a variety of datasets summarized below.
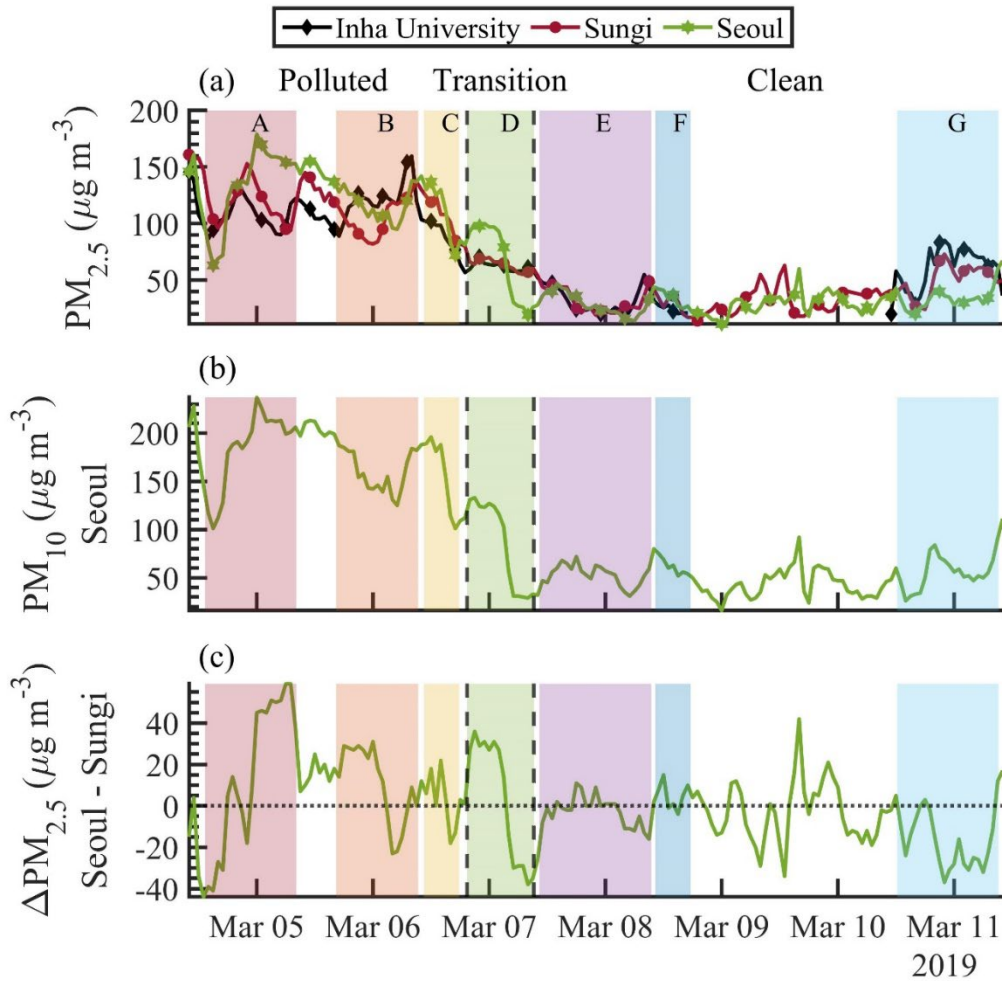
Figure 2. Time series of the following parameters: (a) PM$_{2.5}$ measured at Inha University, Sungi, and Seoul; (b) PM$_{10}$ measured at Seoul; and (c) PM$_{2.5}$ difference between Seoul and Sungi. The dashed black vertical lines separate the (left) polluted, (middle) transition, and (right) clean periods. The horizontal line in (c) denotes a PM$_{2.5}$ difference of zero to clearly show positive and negative deviations from that value. Shaded regions are labeled with individual DLPI+ sets (see Table 2) overlapping in time.

2.1 Aerosol and Gas Monitoring

The focus of this study is on three specific monitoring sites in Incheon and Seoul (~30 km apart), which were compared to a wide network of other stations in those cities to confirm agreement in temporal variability and concentrations. Incheon has a population of 2,936,367 in contrast to Seoul having 9,565,990 (Korea, 2021). The three primary sites include Inha University and Sungi in Incheon, and the Seoul Intensive Monitoring Station (hereafter referred to as Seoul site) in Seoul (locations in Fig. 1). Measurements at these sites are described below and summarized in Table 1. Figure 1 shows the location of the other 17 and 40 National Ambient air quality Monitoring Information System (NAMIS) stations in Incheon and Seoul, respectively, which were operational during the study period with data provided online by AirKorea; Sungi is one of those sites in Incheon but the Inha and Seoul sites are not part of that network. The rationale for including two primary sites in Incheon is because Inha provided unique data not typically measured by NAMIS, and Sungi was closest to Inha among the NAMIS options. The Seoul site had very comprehensive measurements itself and thus it was sufficient for this study.

Table 1. Sample site name, elevation in meters above sea level (MASL), latitude and longitude coordinates of each site, and the parameters measured at each site.

Site	Elevation (MASL)	Latitude	Longitude	Measurements
Incheon: Inha University	23	37°27'2.08"N	126°39'20.87"E	Aerosol: $PM_{2.5}$, 467/528/652 nm wavelength absorption coefficient (α), size-resolved particulate mass samples
Incheon: Sungi	46	37°27'34.74"N	126°39'27.31"E	Aerosol: $PM_{2.5}$ Gas: Ozone (O_3), nitrogen dioxide (NO_2), carbon monoxide (CO), sulfur dioxide (SO_2)
Incheon Meteorological Site	70	37°28'39.85"N	126°37'28.40"E	Meteorological: Ambient temperature (T), wind speed and direction, ambient relative humidity (RH), ambient pressure (P), rain
Seoul Intensive Monitoring Station	30	37°36'38.40"N	126°56'1.36"E	Aerosol: PM_{10}, $PM_{2.5}$; speciated $PM_{2.5}$ concentrations of sulfate (SO_4^{-2}), nitrate (NO_3^-), chloride (Cl^-), sodium (Na^+), ammonium (NH_4^+), potassium (K^+), magnesium (Mg^{2+}), calcium (Ca^{2+}), organic carbon (OC), elemental carbon (EC), silicon (Si), titanium (Ti), vanadium (V), manganese (Mn), iron (Fe), nickel (Ni), copper (Cu), zinc (Zn), Arsenic (As), selenium (Se), lead (Pb) Gas: SO_2, NO_2, O_3, CO Meteorological: T, wind speed and direction, RH, P, rain

2.1.1 Inha University (Incheon)

Aerosol composition measurements were conducted on a building rooftop (23 m ASL; 37° 27' 2.08"N, 126° 39' 20.87"E) on the Inha University campus, which is a residential area ~3 km away from Incheon harbor. Three instruments were operated simultaneously during the study period from 4 March 2019 to 11 March 2019. Real-time $PM_{2.5}$ measurements were conducted using an optical particle counter (OPC-Grimm model 1.109, Grimm Aerosol Technik, Germany) with 1 min time resolution. The OPC measures the number concentration of aerosol particles for 31 channels with size ranging from 0.253 to 31.15 μm, which then get converted into a mass concentration via mathematical extrapolation with a correction factor specific to the Grimm 1177 software. Real-time monitoring of light absorbing aerosol particles was conducted with a tricolor absorption photometer (TAP model 2901, Brechtel Mfg. Inc., USA), which monitors light absorption by particles on a filter at three wavelengths (467, 528, 652 nm). In this study we focus on 652 nm data for simplicity. Lastly, size-resolved particulate matter samples were collected on Teflon filters (PTFE support, 0.1 μm pore, 25 mm, Zefon International) using a low pressure impactor (DLPI+, Dekati, Finland) with aerodynamic lower cutpoint diameters of 0.016, 0.030, 0.054, 0.094, 0.15, 0.25, 0.38, 0.60, 0.94, 1.6, 2.5, 3.6, 5.3, and 10 μm. Daily filter sets were collected on the seven days of the sampling period with details shown in Table 2. Temperature and relative

humidity varied slightly between sets (Table 2) with potential impacts on size of particles owing to hygroscopic growth and evaporation/condensation (e.g., Chen et al., 2018). As temperatures were low (4.5-9.1°C on average), evaporation is likely negligible. There was more potential for hygroscopic growth during the polluted and transition periods (66-79% RH) as compared to the clean period (47-52% RH), and this does not alter conclusions of this work as size shifts owing to water uptake are an important aspect of understanding regional haze events in the study region. Note as well that hygroscopic influence on size cut-off shifts in cascade impactors are most important for RHs above 80% and when sea salt is dominant (Chen et al., 2018), which does not apply to this study. Particles were extracted from the filters in 10 mL of deionized water and placed in ultrasonic bath at 30°C for 60 min for subsequent analysis with ion chromatography (IC, Thermal Scientific Dionex ICS-2100 system) to speciate anions and cations.

Table 2. Summary of the DLPI$^+$ sample sets including sample set name, pollution category, the start and end date in Korea standard time (KST = UTC + 9 hr), as well as the sample averages of T, wind speed and direction, RH, and P. Sample flow rate was 9.71 L min^{-1} for all sample sets.

Set	Pollution Category	Start Time (KST)	End Time (KST)	T (°C)	Wind Speed (m s^{-1})	Wind Direction (°)	RH (%)	P (hPa)
A	Polluted	3/4/2019 13:21	3/5/2019 08:10	7.2	3.0	236	79	1009
B	Polluted	3/5/2019 16:24	3/6/2019 09:19	6.4	1.7	224	74	1010
C	Polluted	3/6/2019 10:32	3/6/2019 17:48	9.1	2.7	307	66	1007
D	Transition	3/6/2019 19:26	3/7/2019 09:15	4.5	3.9	221	75	1008
E	Clean	3/7/2019 10:21	3/8/2019 09:28	5.7	2.9	295	52	1014
F	Clean	3/8/2019 10:19	3/8/2019 17:34	8.9	3.2	244	47	1017
G	Clean	3/10/2019 12:14	3/11/2019 09:08	8.3	2.8	220	51	1002

The IC analysis has been described in other works (Stahl et al., 2020;MacDonald et al., 2018;Cruz et al., 2019), with limits of detection (LOD) for each species examined shown in Table S1. Values measured below the LOD are replaced with LOD/2, with the percent of such samples per species provided in Table S1. For anion analysis, an AS11-HC 250 mm column and potassium hydroxide eluent were used with the following gradient program with a suppressor (AERS 500e) current of 28 mA: begin at 2 mM, increase to 8 mM from 0 to 20 minutes, and then increase from 8 to 28 mM from 20 to 30 minutes. Cation analysis involved a CS12A 250 mm column and methanesulfonic acid eluent with the following program with a suppressor (CERS 500e) current of 22 mA: start at 5 mM, isocratic from 0 to 13 minutes, increase from 5 to 18 mM from 13 to 16 minutes, and then isocratic at 18 mM from 16 to 30 minutes. Sample concentrations were corrected using background sample concentrations for individual species, which included sodium (Na^+), ammonium (NH_4^+), potassium (K^+), magnesium (Mg^{2+}), calcium (Ca^{2+}), chloride (Cl^-), NO_3^-, SO_4^{2-}, methanesulfonate (MSA), adipate, maleate, oxalate, and phthalate. The latter five species were summed in parts of the analysis and referred to as "organic acids" with the caveat that they represent the dissociation anion of either sulfonic or organic acids.

Concentrations for SO_4^{2-}, Mg^{2+}, K^+, and Ca^{2+} refer to their non-sea salt (NSS) values based on calculations relying on the measured concentrations of Na^+ and its ratio with these species in pure sea salt (Seinfeld and Pandis, 2016). The mean percentage of sea salt mass removed for those four species relative to total speciated mass of each filter set (excluding the sea salt portion of those four species) was 2%. Those species for which more than 15% of samples were below the LOD (i.e., Mg^{2+}, maleate, phthalate, adipate, MSA) are not discussed on an individual basis in this study but are used in calculations dependent on the cumulative dataset such as the overall charge balance; the exception is bromide (Br^-), which is fully removed from calculations as it was always below the LOD.

2.1.2 Sungi Site (Incheon)

We use $PM_{2.5}$, O_3, CO, NO_2, and SO_2 data at one hour time intervals collected at Sungi (46 m ASL; 37° 27' 34.74"N, 126° 39' 27.31"E) by NAMIS. These parameters are measured based on the following methods: $PM_{2.5}$ = Beta Attenuation Monitoring (BAM; MetOne Ins.), SO_2 = pulsed ultraviolet fluorescence method, CO = non-dispersive infrared method, NO_2 = chemiluminescent method, O_3 = ultraviolet photometric method. The gases were monitored by Teledyne API products (SO_2 = 100E, NO_2 = 200E, O_3 = 300E, CO = 400E). Of note is that the $PM_{2.5}$ measured at Sungi and Inha University with independent techniques generally agreed well during the study period (Fig. 1) with a coefficient of determination (R^2) of 0.82.

2.1.3 Seoul Intensive Monitoring Station

Gas and aerosol (PM_{10} and $PM_{2.5}$) data are used from the Seoul site (30 m ASL; 37° 36' 38.40"N, 126° 56' 1.36"E), which is independent from the NAMIS network. The following parameters were measured: $PM_{2.5}$ and PM_{10} = Beta Attenuation Monitoring (BAM), ionic species concentrations (SO_4^{2-}, NO_3^-, Cl^-, Na^+, NH_4^+, K^+, Mg^{2+}, Ca^{2+}) = Ambient Ion Monitor (URG 9000D, URG Co.) and ion chromatography (Dionex, DX-1 000; IonPac AS14A and the CS12A columns), organic carbon (OC) and elemental carbon (EC) = semi-continuous OC/EC analyzer (Sunset Laboratory) based on the thermal/optical reflectance (TOR) method, elemental concentrations (Si, Ti, V, Mn, Fe, Ni, Cu, Zn, As, Se, Pb) = online X-ray fluorescence (XRF) analyzer (Xact-420, Cooper Environmental Co.), SO_2 = pulsed ultraviolet fluorescence method, CO = non-dispersive infrared method, NO_2 = chemiluminescent method, O_3 = ultraviolet photometric method. Gases were monitored with the same techniques as at the Sungi site. All speciated aerosol information at Seoul are for $PM_{2.5}$.

2.2 Meteorological data

Meteorological data for winds, temperature (T), pressure (P), relative humidity (RH), and rain were used from monitoring stations in Incheon and Seoul. The Korea Meteorology Administration provided data from an Automated Synoptic Observing System (ASOS) for the Incheon station (70 m ASL; 37° 28' 39.85"N, 126° 37' 28.40"E) (kma.go.kr), which is located ~5 km northwest of the Inha University sampling site. Meteorological data were collected at the same site described for Seoul in Sect. 2.1.3. Specific humidity (q) was calculated using measured values of T, P, and RH (Bolton, 1980).

Planetary boundary layer height (PBLH) data are used from Modern Era Retrospective-analysis for Research and Application version 2 (MERRA-2) (Gelaro et al., 2017). MERRA-2 uses the Goddard Earth Observing System Data Assimilation System Version 5 (GEOS-5) and is hosted and maintained by the National Aeronautics and Space Administration (NASA) Global Modeling and Assimilation Office (GMAO). The MERRA-2 PBLH product is provided as part of the surface flux diagnostics dataset (GMAO, 2015). The resolution of the PBLH product is 0.5° x 0.625° and is assimilated on an hourly timescale. All four sample sites described above are within the same grid point (37.500°N, 126.875°E) in the MERRA-2 PBLH product.

2.3 Trajectory and Chemical Transport Modeling

We use the NOAA HYSPLIT model (Rolph et al., 2017;Stein et al., 2015) for air mass back-trajectory information. We rely on the Global Data Assimilation System (GDAS) at 0.5° × 0.5° resolution and the model vertical velocity method for treating vertical motion. Four day back-trajectories were calculated for each hour between 4 – 11 March 2019. We use an ending altitude of 500 m AGL at the Inha University sampling site, which was sufficient to represent the predominant sources impacting the various sample sites during the week of focus owing to their close proximity. This ending altitude has proved to be successful for other surface air quality studies in other regions (e.g., Aldhaif et al., 2021;Crosbie et al., 2014;Mora et al., 2017;Hersey et al., 2015) and nearby in southeast Asia (e.g., AzadiAghdam et al., 2019). We obtained data for the following parameters along trajectories: ambient temperature (°C), rainfall (mm hr^{-1}), mixed layer depth (m), RH (%), and downward solar radiation flux (W m^{-2}).

For large-scale background aerosol information we rely on the Navy Aerosol Analysis and Prediction System (NAAPS) (Lynch et al., 2016) accessible at https://www.nrlmry.navy.mil/aerosol/. We specifically use the reanalysis version of NAAPS, called NAAPS-RA. This is a chemical transport model with 25 vertical levels using a terrain-following sigma-pressure coordinate system that provides data in 1° × 1° grids every 6 hours. The model is driven by the Navy Global Environmental Model (NAVGEM) for meteorological information (Hogan et al., 2014). The final reanalysis results are created after assimilating Moderate Resolution Imaging Spectroradiometer (MODIS) and Multi-angle Imaging Spectro Radiometer (MISR) data into the model (Zhang and Reid, 2006;Hyer et al., 2011). Reanalysis output is provided for dust, sea salt, open biomass burning smoke, and "anthropogenic and biogenic fine (ABF)" that includes secondarily produced species (i.e., SO_4^{2-} and SOA) and primary organic aerosols mainly confined to the fine mode (< 1 μm).

3 Time Series of PM Concentrations

March 2019 was characterized by a major transboundary pollution event impacting the Korean peninsula with visual satellite imagery (Fig. S1) clearly showing the presence and then absence of significant haze. Owing to their proximity to one another, the Inha and Sungi stations in Incheon revealed similar values and changes in $PM_{2.5}$ ($R^2 = 0.82$ for the full study period) with a significant reduction from polluted (~115 $\mu g\ m^{-3}$) to transition (~63 $\mu g\ m^{-3}$) and clean (~40 $\mu g\ m^{-3}$) periods (Table 3 and Figs. 1-2). Both Inha and Sungi $PM_{2.5}$ levels were strongly correlated with the mean of data from 17 NAMIS stations across Incheon (Fig. 1: R^2 of 0.82 and 0.98, respectively).

Table 3. Average Incheon meteorological, aerosol, and gas parameters for the polluted, transition, and clean time periods, with standard deviations shown in parentheses. Speciated concentrations from Inha represent mass for particles with diameters above 0.016 µm (i.e., full size range of DLPI$^+$ sampler) and are weighted by sample duration when calculating the time period average; species with concentrations below their respective LOD in more than 50% of samples (see Table S1) are not shown. Standard deviations are not shown for the transition period speciated data owing to there only being one sample set.

Site	Parameter	Polluted	Transition	Clean
Incheon Meteorological Site	T (°C)	7.5 (2.1)	4.7 (1.0)	6.7 (3.2)
	Wind Speed (m s^{-1})	2.5 (0.9)	3.7 (1.3)	2.6 (1.2)
	Wind Direction (°)	247 (45)	236 (150)	219 (126)
	RH (%)	73 (15)	77 (8)	51 (20)
	q (g kg^{-1})	4.63 (0.61)	4.07 (0.64)	2.95 (0.81)
	P (hPa)	1009 (2)	1008 (1)	1011 (5)
	PBLH (km)	0.45 (0.56)	1.87 (1.28)	0.53 (0.63)
	Rain (mm)	0 (0)	0 (0)	0 (0)
Inha University	$PM_{2.5}$ ($\mu g\ m^{-3}$)	110 (17.9)	61.8 (3.9)	43.6 (20.7)
	α (Mm^{-1})	18.9 (5.1)	11 (1.9)	8.6 (3.1)
	NO_3^- ($\mu g\ m^{-3}$)	32.2 (12.1)	10.3 (-)	3.2 (1.1)
	NH_4^+ ($\mu g\ m^{-3}$)	19.2 (7.7)	8.2 (-)	5.6 (3.8)
	SO_4^{2-} ($\mu g\ m^{-3}$)	15.4 (5.2)	7.0 (-)	1.8 (0.6)
	K^+ ($\mu g\ m^{-3}$)	0.7 (0.3)	0.7 (-)	0.2 (0.05)
	Ca^{2+} ($\mu g\ m^{-3}$)	2.0 (0.4)	1.9 (-)	1.7 (0.6)
	Cl^- ($\mu g\ m^{-3}$)	2.0 (1.1)	1.6 (-)	0.8 (0.1)
	Na^+ ($\mu g\ m^{-3}$)	1.1 (0.2)	1.5 (-)	0.8 (0.1)
	Oxalate ($\mu g\ m^{-3}$)	0.7 (0.4)	0.3 (-)	0.2 (0.01)
Sungi	$PM_{2.5}$ ($\mu g\ m^{-3}$)	117.3 (20.5)	64.6 (6.6)	36.2 (14.1)
	CO (ppb)	927 (197)	800 (68)	578 (154)
	NO_2 (ppb)	45 (19)	32 (14)	37 (16)
	O_3 (ppb)	37 (16)	31 (11)	27 (16)
	SO_2 (ppb)	7 (2)	6 (1)	8 (4)

Meanwhile, ~30 km farther inland at Seoul, both PM_{10} and $PM_{2.5}$ dropped at a similar rate as Incheon between the three periods (Table 4 and Figs. 1-2): PM_{10} = ~176 $\mu g\ m^{-3}$, ~91 $\mu g\ m^{-3}$, ~50 $\mu g\ m^{-3}$; $PM_{2.5}$ = ~127 $\mu g\ m^{-3}$, ~71 $\mu g\ m^{-3}$, ~31 $\mu g\ m^{-3}$. The Seoul site $PM_{2.5}$ data were strongly correlated with the 40 NAMIS stations

284 across Seoul (Fig. 1: $R^2 = 0.96$). Based on the three period averages, Seoul exhibited slightly higher $PM_{2.5}$ levels
285 in the polluted and transition periods whereas Incheon was higher during the clean period. The time series of
286 hourly PM data in Figs. 1-2 show that near the end of the clean period there was an increase in pollution levels,
287 which is consistent with HYSPLIT data showing back-trajectories shifting from northerly for most of the clean
288 period to northwesterly (i.e., from the Beijing area) (Fig. 3). The R^2 value between $PM_{2.5}$ hourly data was 0.75
289 and 0.82 for Seoul-Inha and Seoul-Sungi, respectively. Although there was decent agreement, differences are
290 apparent in the $PM_{2.5}$ hourly time series (Fig. 2c) with Seoul's levels being significantly enhanced during parts
291 of the polluted and transition periods. The difference in $PM_{2.5}$ between Seoul and Incheon suggests enhanced
292 local production promoting large differences between hourly $PM_{2.5}$ over Seoul versus Incheon. For example, the
293 maximum/mean ± standard deviation in the $PM_{2.5}$ difference (μg m^{-3}) between Seoul and Sungi were as follows
294 for the three periods: polluted = 59/10 ± 26; transition = 36/6 ± 28; clean = 42/-6 ± 14.

295
296 **Table 4. Average meteorological, aerosol, and gas parameters for the polluted, transition, and clean time**
297 **periods measured at the Seoul sampling site, with standard deviations shown in parentheses. Note that**
298 **organic aerosol (OA) concentration was calculated by multiplying the OC concentration by a factor of 1.8**
299 **(i.e., OA = OC × 1.8).**

Parameter	Polluted	Transition	Clean
T (°C)	9.3 (3.0)	5.7 (2.0)	7.6 (4.2)
Wind speed (m s^{-1})	1.9 (0.8)	1.8 (1.0)	1.6 (1.0)
Wind direction (°)	240 (59)	261 (104)	178 (128)
RH (%)	55 (17)	69 (5)	36 (14)
q (g kg^{-1})	3.80 (0.66)	3.87 (0.31)	2.17 (0.64)
P (hPa)	1018 (3)	1016 (1)	1019 (5)
PBLH (km)	0.45 (0.56)	1.87 (1.28)	0.53 (0.63)
Rain (mm)	0 (0)	0 (0)	0 (0)
PM_{10} (μg m^{-3})	176.0 (35.0)	90.8 (43.8)	50.3 (16.6)
$PM_{2.5}$ (μg m^{-3})	127.2 (27.5)	70.6 (32.5)	30.5 (9.9)
PM_{10}/$PM_{2.5}$	1.39 (0.09)	1.27 (0.12)	1.69 (0.38)
NO_3^- (μg m^{-3})	43.3 (12.0)	17.3 (9.1)	7.1 (3.4)
NH_4^+ (μg m^{-3})	21.7 (5.0)	11.1 (5.2)	3.2 (1.3)
SO_4^{2-} (μg m^{-3})	19.8 (4.2)	12.3 (5.7)	2.5 (1.3)
OA (μg m-3)	17.0 (3.9)	15.3 (5.6)	10.0 (3.4)
OC (μg m^{-3})	9.4 (2.1)	8.5 (3.1)	5.6 (1.9)
EC (μg m^{-3})	2.9 (0.7)	2.2 (0.8)	1.2 (0.5)
Cl^- (μg m^{-3})	1.4 (0.6)	0.7 (0.3)	0.5 (0.2)
K^+ (μg m^{-3})	0.3 (0.1)	0.2 (0.1)	0.12 (0.05)
Ca^{2+} (μg m^{-3})	0.2 (0.1)	0.08 (0.04)	0.07 (0.03)
Na^+ (μg m^{-3})	0.12 (0.04)	0.04 (0.02)	0.05 (0.03)
Mg^{2+} (μg m^{-3})	0.08 (0.01)	0.03 (0.02)	0.02 (0.02)
Fe (ng m^{-3})	447 (94)	243 (125)	185 (70)
Si (ng m^{-3})	422 (201)	222 (131)	84 (72)
Zn (ng m^{-3})	113 (40)	47 (22)	47 (33)
Pb (ng m^{-3})	42 (10)	34 (17)	15 (7)
Mn (ng m^{-3})	28 (7)	14 (8)	10 (5)
Ti (ng m^{-3})	23 (6)	13 (6)	10 (3)
Cu (ng m^{-3})	14 (7)	6 (3)	8 (6)
V (ng m^{-3})	8 (5)	3 (2)	1 (1)

As (ng m^{-3})	7 (2)	8 (6)	3 (2)
Se (ng m^{-3})	4 (1)	2 (1)	1 (1)
Ni (ng m^{-3})	3 (2)	1 (1)	0.5 (0.5)
CO (ppb)	1104 (175)	1036 (145)	655 (139)
O$_3$ (ppb)	38 (18)	29 (12)	23 (16)
NO$_2$ (ppb)	37 (14)	30 (13)	38 (16)
SO$_2$ (ppb)	7 (1)	5 (0)	6 (2)

300
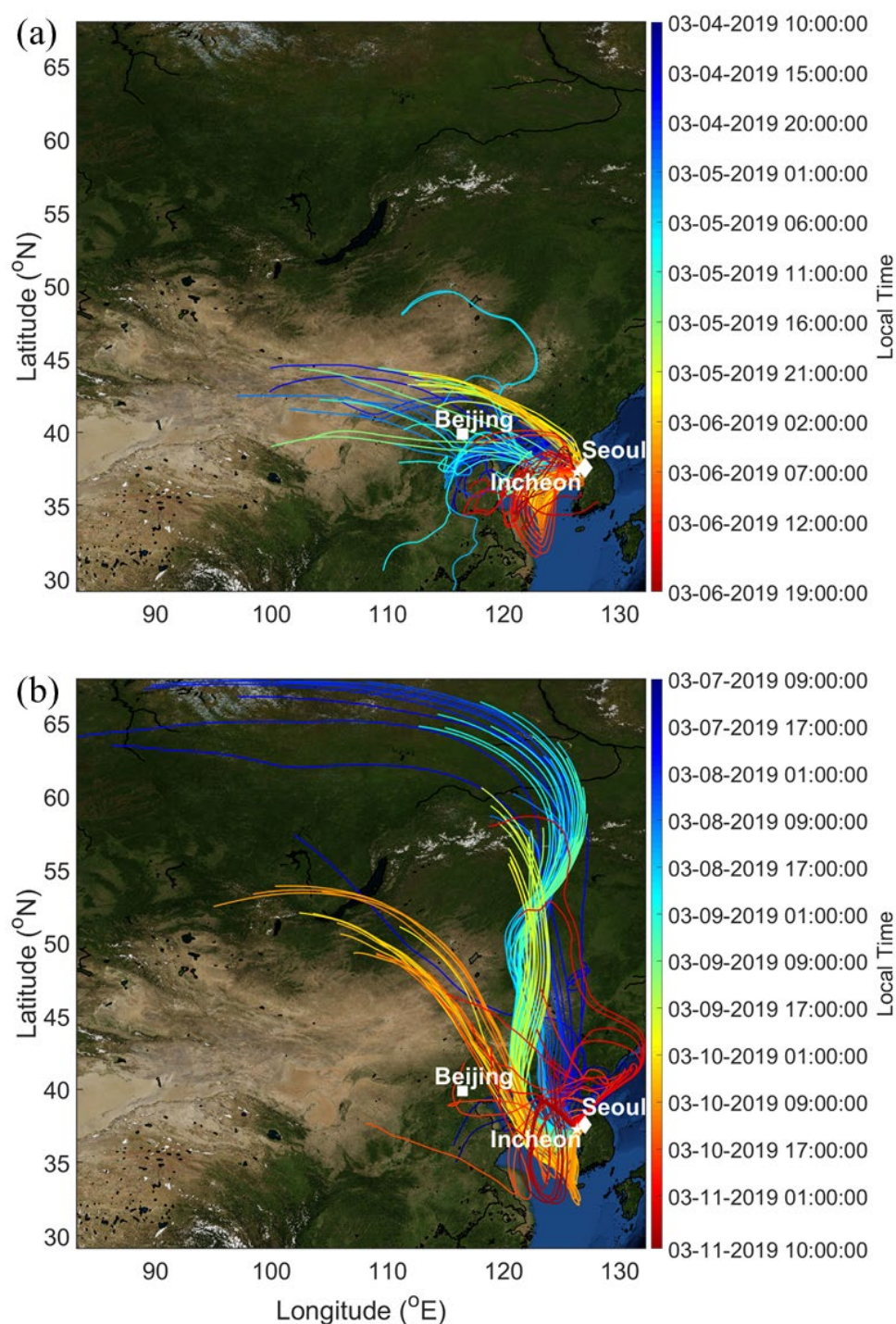
Figure 3. Four-day back-trajectories based on hourly data during the (a) polluted and (b) the clean portion of the study period. The ending point of trajectories is at 500 m AGL at Incheon, with environmental parameters along the trajectories summarized in Fig. S4. Images retrieved from https://worldview.earthdata.nasa.gov/.

The PM_{10}:$PM_{2.5}$ ratio is helpful to examine whether a divergence in values occurs that would suggest a strong source of dust as compared to typical background conditions. More specifically, higher values of this ratio could potentially suggest enhanced dust influence owing to mass concentrations of dust being abundant above 2.5 μm. As PM_{10} was only measured at Seoul, Table 4 compares the mean (± standard deviation) value of this ratio for the three time periods: polluted = 1.39 ± 0.09, transition = 1.27 ± 0.12, clean = 1.69 ± 0.38. As will be discussed

312 more subsequently, dust did not drive the high PM concentrations during the polluted period, but rather it was
313 driven in large part by secondarily produced species (i.e., SO_4^{2-}, NO_3^-, NH_4^+) that grew into the $1 - 2.5$ μm range.
314
315 **4 PM Composition**
316 **4.1 $PM_{2.5}$ Composition**
317   Speciated $PM_{2.5}$ data from Seoul (Table 4) reveal that the largest contributor was NO_3^- during the
318 polluted and transition periods, with an average concentration during the polluted period of 43.3 μg m^{-3}.
319 Estimating OA mass from the measured mass concentration of OC (OA [μg m^{-3}] = 1.8 × OC [μg m^{-3}] (Zhang et
320 al., 2005)) indicates that OA dominated the $PM_{2.5}$ mass during the clean period followed by NO_3^-. Of all species
321 measured in Table 4, SO_4^{2-} exhibited the highest relative enhancement during the polluted period versus the
322 clean period (factor of 7.9), whereas NH_4^+ and NO_3^- were enhanced by factors of 6.8 and 6.1, respectively. OA
323 was only enhanced by a factor of 1.7. In terms of mass concentrations, the difference between the polluted and
324 clean periods for the sum of nitrate, sulfate, and ammonium was 72 μg m^{-3} versus the difference in OA of 7 μg
325 m^{-3} (Table 4). The change in OA is < 10% of the change in the three major inorganic ions.
326   The strong enhancement of the inorganic constituents owes most likely to rapid production (both
327 locally and in transport) in contrast to transported PM that was already produced upwind; the latter would tend
328 to increase OA along with inorganic constituents more comparably than what was observed. In lesser abundance
329 were Cl^-, Na^+, K^+, Mg^{2+}, and Ca^{2+}, which are linked to sea salt and dust (Seinfeld and Pandis, 2016) and thus
330 expected to have appreciable concentrations above 2.5 μm. In terms of the elemental species, the most prevalent
331 species in all three periods were the crustal tracer species Si and Fe, which were 5.0 and 2.4 times higher in
332 concentration, respectively, during the polluted period versus the clean period (Table 4). Most of the crustal
333 tracer species showed enhancements ranging from $1.8 - 2.8$. Only Si, Se, and V showed greater enhancement
334 ratios with the latter two enhanced by factors of 4 and 8, respectively.
335   The sum of the $PM_{2.5}$ components using OC in Table 4 accounted for 79% (polluted), 75%
336 (transition), and 68% (clean) of the total $PM_{2.5}$, which is partly due to unmeasured species and that OC includes
337 only the carbon mass and not other elements associated with organic compounds. Using OA instead of OC
338 yields improved $PM_{2.5}$ closure: 85% (polluted), 85% (transition), 83% (clean). This decent level of closure may
339 be largely attributed to the high relative abundance of more easily measured inorganic species, predominantly
340 NO_3^-, SO_4^{2-}, and NH_4^+.
341
342 **4.2 Mass Size Distributions**
343   The mass size distribution measurements in Incheon provide a unique look into a typical transboundary
344 pollution event, with the ability to contrast it to the subsequent transition and clean periods. Insights gathered from
345 this analysis have direct relevance to Seoul owing to close proximity to Incheon (~30 km) with the exception of
346 any additional aerosol processing and formation that took place between Incheon and Seoul, including especially
347 Seoul itself. Charge balance details can be found in Sect. S1 and Fig. S2, with a general anion deficit during the
348 study period, including anions not speciated with the IC technique such as various types of organics.
349   Figure 4 summarizes size-resolved composition for the polluted, transition, and clean periods of this
350 study. Ions typically associated with primary natural aerosol sources such as sea salt and dust (Arimoto et al.,
351 1992;Seinfeld and Pandis, 2016), including Ca^{2+}, Na^+, and Cl^-, did not exhibit any significant enhancement during
352 the polluted period (cumulative mass concentrations in Table 3), with varying size distribution peaks based on the
353 species and period during the study. In contrast, the ions linked to secondary formation via gas-to-particle
354 conversion processes (i.e., SO_4^{2-}, NO_3^-, NH_4^+, and organic acids) were dramatically enhanced during the polluted
355 period compared to the clean period (Fig. 4) with the transition in between. These species exhibited their highest
356 concentrations during the polluted period between 0.38 and 3.60 μm, a range which includes larger sizes for these
357 secondarily produced species (especially SO_4^{2-} and NH_4^+) as compared to other regions where their peaks are
358 reported to be between 0.3 and 0.6 μm (Maudlin et al., 2015;Cruz et al., 2019). During the transition period, the
359 inorganic species exhibited maximum concentrations for particles with diameters between 0.38 and 1.60 μm. The
360 clean period was generally marked by these species exhibiting peak concentrations for particles between 0.25 and
361 0.38 μm with a secondary peak from 0.6 and 0.94 μm, albeit neither is pronounced.
362   The likely formation pathway for SO_4^{2-}, NO_3^-, NH_4^+, and organic acids in the polluted period was
363 secondary production, which was assisted in part by high humidity as discussed in more detail in Sect. 6.2. Their
364 common formation mechanism is supported by significant correlations (r ≥ 0.94; see time series in Fig. S5) during
365 the polluted period between SO_4^{2-}, NO_3^-, NH_4^+, and oxalate, with the latter being the most abundant organic acid
366 during the entire study period but especially in the polluted period (~70% of organic acid mass). Oxalate is
367 produced efficiently via aqueous-phase chemistry (Sorooshian et al., 2007;Sorooshian et al., 2006;Wonaschuetz
368 et al., 2012). The strong correlation between oxalate and SO_4^{2-} during the polluted period is important as a strong

correlation between these species (in the absence of biomass burning) is considered a marker for secondary aqueous aerosol formation (Ervens et al., 2004;Yu et al., 2005;Zhou et al., 2015;Hilario et al., 2021a). The fact that oxalate exhibits a greater enhancement ratio in Table 3 than that of OA in Table 4 is not surprising since not all OA is produced via aqueous processing and even components that are may be produced at different rates. Thus, it is cautioned that oxalate is not a good proxy for OA overall in haze.
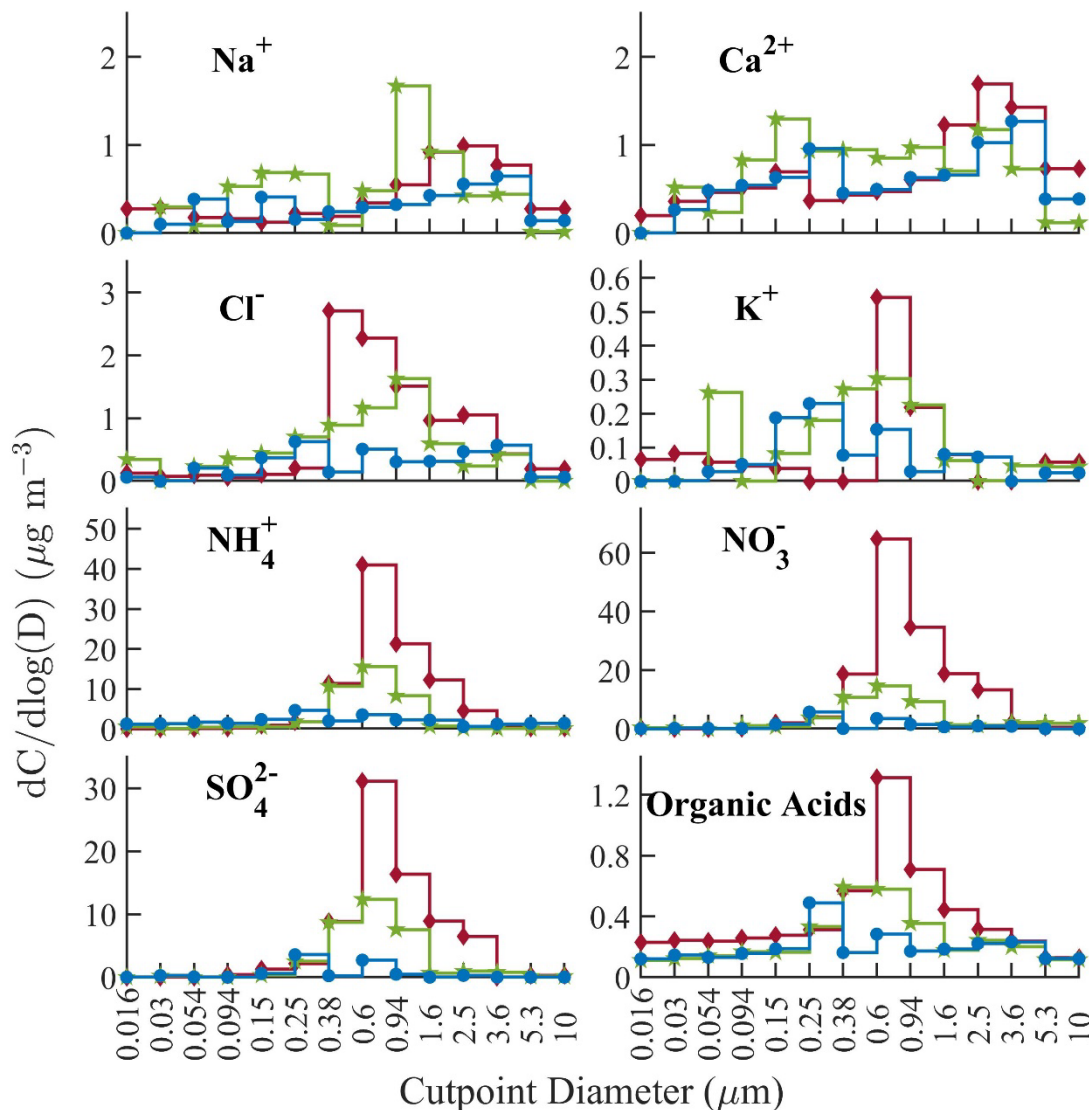
Figure 4. Size-resolved composition dC/dlog(D) for (red) polluted, (green) transition, and (blue) clear sample periods. Organic acids = sum of MSA, adipate, maleate, oxalate, phthalate. Sample set data were weighted by sample duration for the polluted and clean periods (note: transition period had just one set). Species that were below LOD in more than 50% of samples (see Table S1) are not shown.

We next examine if NH_3 was completely neutralized by HNO_3 and H_2SO_4. A charge balance between SO_4^{2-}, NO_3^-, and NH_4^+ can indicate complete neutralization with a slope of unity, as has been tested by other studies (e.g., Lee et al., 2003). A charge balance using individual stages of the three polluted sets collected at Inha University (NH_4^+ on y-axis) between these three species (Fig. S3) yielded a best-fit line slope and y-intercept of 1.34 and −0.02, respectively (R^2 = 0.99, n = 20). Our data reveal an anion deficit and that there was sufficient NH_3 to fully neutralize HNO_3 and H_2SO_4. Furthermore, there likely was limited interaction of these acidic gases with coarse particles (e.g., dust and sea salt) that were relatively low in abundance.

5 Regional Conditions Influencing PM

5.1 Atmospheric Circulation and Meteorology

According to previous meteorological analysis (Park et al., 2020a), the airmass history for the polluted period was influenced by the interaction between a Siberian high-pressure system and a migratory anticyclone system, which were located over the Korean peninsula. From 28 February to 1 March 2019, a high-pressure system was located to the west and low-pressure systems were located to the east, all conspiring to yield westerly and northwesterly winds. Lee et al. (2019a) examined a similar time period (27 February – 7 March 2019) and suggested that pollution between 3 – 5 March was transported to the Seoul area at low and high altitudes from the Shandong Peninsula and Beijing, respectively. Pollution levels were exacerbated over South Korea due to a weak high pressure system lingering over the Korean peninsula between 2 and 5 March (Park et al., 2020a). This is evident from the HYSPLIT back-trajectories (Fig. 3a) showing airmasses moving slower in the polluted period versus the subsequent clean period (Fig. 3b). Following the lingering period, a low-pressure system moved in over Russia associated with more clouds and rain upwind of the sampling sites (Fig. S4). There were stronger winds that were northerly between 7 and 11 March. In both the polluted and clean periods, air masses descended from ~2.5 – 4 km four days earlier to within the mixing layer (Fig. S4). The NAAPS spatial maps of speciated optical depths (Fig. S6) and surface mass concentrations (Fig. S7) confirm the spatial extent of the regional haze event extending from the Korean peninsula to areas like Beijing with the ABF (Anthropogenic and Biogenic Fine = SO_4^{2-}, primary organic aerosols, and SOA) component being most prominent during the study period and the driver of the polluted period enhancements in PM, consistent with the dominance of SO_4^{2-}, NO_3^-, and NH_4^+ from the in-situ measurements.

The local weather conditions at both Incheon (Table 3) and Seoul (Table 4) exhibited the following common characteristics: (i) generally low average temperatures (< 10°C) that decreased after the polluted period; (ii) low average wind speeds (2.5 – 3.7 m s^{-1} in Incheon, < 2 m s^{-1} in Seoul); iii) highest mean PBLH during the transition period (1.87 km compared to ≤ 0.53 km for the other periods); (iii) lowest average humidity in the clean period (RH ≤ 51% and q ≤ 2.95 g kg^{-1}); and (iv) negligible rain. Although locally there was negligible rain, there was some precipitation along the trajectories arriving at these sites in the polluted and clean periods (Fig. S4), with some potential to reduce aerosol concentrations via wet removal. The time series of these various environmental conditions at Incheon and Seoul (Fig. S8) demonstrate high temporal similarity and the similar characteristics noted above. The relatively low regional wind speeds during the polluted period (Figs. 3 and S8) indicate that transport was slow allowing for the accumulation and persistence of the haze over this whole domain.

5.2 Gas Concentrations

Gases (CO, O_3, NO_2, SO_2) exhibited fairly similar values (Tables 3-4) and temporal patterns (Fig. S9) between Sungi and Seoul, with CO exhibiting the largest relative reduction between successive periods, followed by O_3. $PM_{2.5}$ only exhibited a strong relationship with CO at Sungi and Seoul based on correlation coefficients during the full study period (r = 0.84 and 0.87, respectively). As CO is a tracer for anthropogenic emissions (Fishman and Seiler, 1983), its high correlation with $PM_{2.5}$ at both sites supports the strong influence of anthropogenic aerosol at both sites. The reduction of CO from the polluted to the clean period is possibly due to Chinese influence; in contrast to South Korea, combustion efficiency has been shown to be worse in China (Halliday et al., 2019), which supports the high CO levels during the polluted period with air masses coming from China. Carbon monoxide concentrations in Seoul exceeded Incheon by 177 ppb on average during the polluted period, suggestive of added influence from local emissions in Seoul superimposed on top of the transported pollution. Carbon monoxide is commonly used in calculations related to aerosol transport studies (e.g., Dadashazar et al., 2021;Hilario et al., 2021b) as it is relatively insensitive to wet scavenging processes with a long lifetime in the atmosphere (~1 month) compared to aerosol particles (Weinstock, 1969).

6 Evidence for Enhanced Local Secondary Aerosol Production

6.1 Differences Between Seoul and Incheon

We now consider $PM_{2.5}$ differences between Incheon and Seoul, where the latter exhibits elevated levels during most of the polluted period (Fig. 2). KORUS-AQ research highlighted that while transport brings aerosol particles from upwind sources, high humidity and cloudiness concentrates local pollution in a shallow stable boundary layer, which promotes secondary aerosol production (Jordan et al., 2020). Jordan et al. (2020) showed that Seoul exhibited $PM_{2.5}$ levels that were on average ~10 μg m^{-3} higher than those at Incheon during the transport/haze period of KORUS-AQ that persisted for 7 days. The maximum daily mean enhancement of $PM_{2.5}$ in Seoul from Incheon over that period was 24 μg m^{-3}, while the peak hourly mean enhancement reached 32 μg m^{-3}. These observations were attributed plausibly to more local emissions in Seoul. The same explanation arguably applies to a large extent in our study period too, where the mean difference during the polluted period between

Seoul and Incheon PM$_{2.5}$ was 10 µg m^{-3} for Sungi and 17 µg m^{-3} for Inha (Tables 3 and 4) with the peak hourly enhancement between Seoul and Sungi being nearly 60 µg m^{-3} (Fig. 2). Here again, humidity (both q and RH) is elevated and PBLH is low compared to the subsequent clean period when PM levels were drastically lower. As the two sites are quite close to one another (~ 30 km), the most likely explanation for higher PM levels at Seoul is more local emissions rather than additional aging to produce secondary aerosol species via transport.

6.2 Role of Humidity

One finding of this work is the significant amount of secondarily produced species in the supermicrometer range. More specifically, the relative fraction of SO$_4^{2-}$, NO$_3^-$, NH$_4^+$, and organic acids in the supermicrometer range (i.e., technically D ≥ 0.94 µm) as compared to all sizes sampled at Inha (D ≥ 0.016 µm) during the polluted period was 43%, 44%, 42%, and 36%, respectively, which is appreciable and potentially influenced by the humid conditions. More specifically, it is hypothesized that in the polluted period there was both hygroscopic growth of particles and additional chemical uptake in those swollen particles with enhanced aerosol-laden water to promote higher concentrations of these secondary species.

Of the meteorological parameters shown in Tables 3-4, PM$_{2.5}$ levels at Inha University, Sungi, and Seoul were best correlated with q (r = 0.66, 0.64, and 0.78, respectively) across the entire study period. The second-best relationship was with RH (r = 0.53, 0.47, and 0.53, respectively) with minimal relationships with either temperature (r: 0.02 – 0.17) or wind speed (-0.29 ≤ r ≤ 0.13). This motivates an examination of the relationships between PM and humidity to assess the plausibility of a role for heterogeneous secondary aerosol production from local and transported gas-phase precursors.

One metric used to quantify such enhanced aerosol production is the oxidation ratio, specifically the sulfur and nitrogen oxidation ratios (SOR and NOR, respectively) where SOR = SO$_4^{2-}$/(SO$_4^{2-}$ + SO$_2$) and NOR = NO$_3^-$/(NO$_3^-$ + NO$_2$) (Colbeck and Harrison, 1984). Higher values of SOR and NOR indicate that the gaseous precursors form higher relative amounts of SO$_4^{2-}$ and NO$_3^-$, respectively (Kaneyasu et al., 1995). Previous studies have reported increased SOR and NOR as a function of RH at several locations throughout China including Nanjing, Beijing, Hangzhou, and Xi'an (Zhang et al., 2021;Quan et al., 2015;Wu et al., 2018;Huang et al., 2020;Ji et al., 2018). In particular, Huang et al. (2020) showed that SOR increased exponentially with aerosol water content when RH > 50% in Beijing during polluted periods in the wintertime. Given our finding that q is better correlated with PM$_{2.5}$ than RH, we compare SOR and NOR to q (Fig. 5). We evaluate these ratios for Seoul data only as all the requisite data were measured at the same site. The mean (± standard deviation) of NOR during the three time periods of the study was as follows: polluted = 0.39 ± 0.1; transition = 0.22 ± 0.10; clean = 0.09 ± 0.04. Similarly, the mean (± standard deviation) of SOR was as follows: polluted = 0.51 ± 0.06; transition = 0.44 ± 0.14; clean = 0.14 ± 0.07. We find a positive relationship between NOR and SOR with q(RH), with R^2 values being 0.58(0.24) and 0.82(0.43), respectively. For context, during a polluted period in Xi'an, China, NOR and SOR values were 0.32 and 0.33, respectively, with high R^2 values with aerosol water content (NOR = 0.55; SOR = 0.81) (Zhang et al., 2021). While the average q and RH were slightly higher for the transition period in Seoul relative to the polluted period (Table 4), the peak values of q, RH, SOR, and NOR all occurred during the beginning of the polluted period (Fig. S10).

This study's results suggest there was significant heterogeneous processing to produce species like SO$_4^{2-}$, NO$_3^-$, NH$_4^+$, and organic acids above ~1 µm. These species accounted for ~93% of the total speciated ion mass at Inha during the polluted period (Table 3) and are strongly correlated with one another (0.93 ≤ r ≤ 1.00). Heterogeneous production of inorganic species such as SO$_4^{2-}$ in cloudy and humid conditions is common for the study region (Jeon et al., 2021;Jordan et al., 2020;Park et al., 2020b). Furthermore, significant secondary production of SO$_4^{2-}$ above 1 um at high RH has been noted in Beijing (Wang et al., 2020). Mechanisms potentially responsible include aqueous oxidation by O$_3$, H$_2$O$_2$, and transition-metal ion-catalyzed O$_2$, and also heterogeneous oxidation on surfaces of aerosol particles and droplets via the same oxidants (Li et al., 2020). Table 4 shows that at Seoul the concentrations of elements such as Fe, Cu, Zn, and Pb were higher during the polluted period, which is assumed to be similar at Incheon, supporting the possibility of transition metal-catalyzed secondary production of secondary SO$_4^{2-}$. Enhanced aerosol liquid water in more humid conditions also promotes partitioning of species to the aerosol-phase as has been documented for NO$_3^-$ in the study region (Seo et al., 2020) and is common for organic acid precursors (Hennigan et al., 2008;Hennigan et al., 2009;Sorooshian et al., 2010). The increased total concentration of NH$_4^+$ in the polluted period relative to the clean period and strong correlation with SO$_4^{2-}$, NO$_3^-$, and oxalate is related to its key role in salt formation (Paciga et al., 2014;Seinfeld and Pandis, 2016;Zhang et al., 2015).
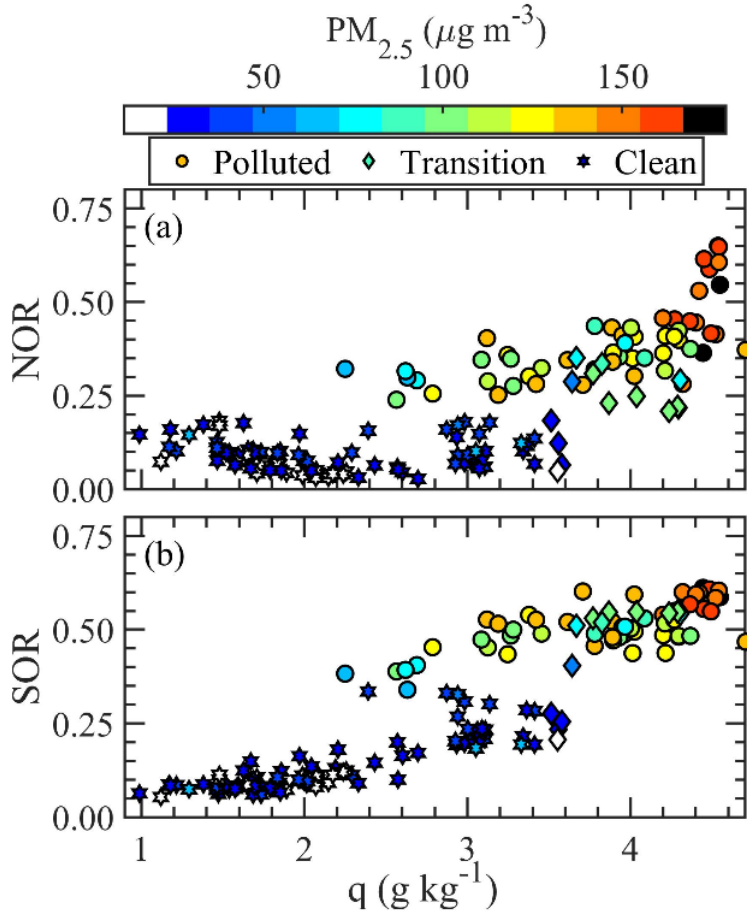
Figure 5. (a) Nitrogen oxidation ratio (NOR) and (b) sulfur oxidation ratio (SOR) as a function of q based on hourly Seoul data. Points are colored by PM$_{2.5}$ with shapes assigned to the three time periods in the study.

6.3 Does PM$_1$ Composition Represent PM$_{2.5}$ Composition?

The size-resolved composition data in Incheon allows for a comparison of how the composition of PM$_{0.94}$ differs from the fraction of remaining material contributing to PM$_{2.5}$ (denoted PM$_{2.5-0.94}$). Figure 6 shows that while the transition and clean periods exhibit differences between the apportionment of the mass between PM$_{0.94}$ and PM$_{2.5-0.94}$, during the polluted period the composition is essentially the same. This supports the argument that the presence of supermicrometer secondary inorganic species derives from the same processes the give rise to those compounds in PM$_{0.94}$. Hence, composition measurements using instruments that exclude supermicrometer particles can be used to investigate the composition and evolution of East Asian haze events. Further, models can reliably apply PM$_1$ composition apportionment to the full PM$_{2.5}$ size range in their assessments of sources and mitigation strategies for these events. A cautionary note is that these implications apply when PM is dominated by inorganics, as with our case, with a limitation of our analysis being the lack of comprehensive size-resolved OC measurements. However, the differences evident in the transition and clean periods imply that under other atmospheric conditions PM$_1$ composition measurements will not fully reflect the apportionment of PM$_{2.5}$ aerosols. Another important conclusion from Fig. 6 is that the relative amount of PM$_{2.5-0.94}$ versus PM$_{0.94}$ was highest in the polluted period (39% of speciated PM$_{2.5}$ vs. 28% for transition and 21% for clean), further reinforcing that there was increased production of secondarily formed inorganic species in the coarse mode.
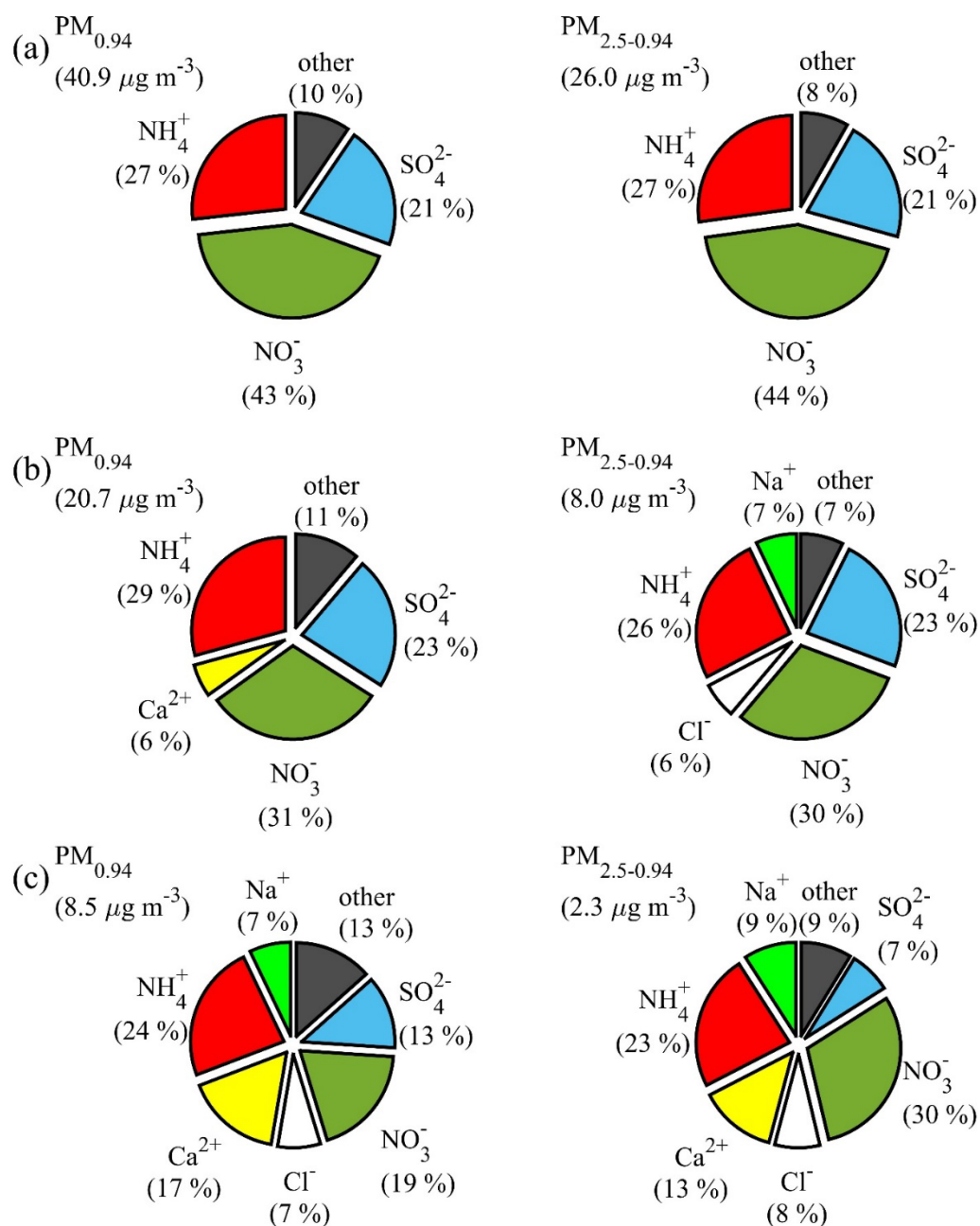
Figure 6. Percent composition of (left panels) PM$_{0.94}$ and (right panels) particulate mass between 0.94 and 2.50 μm (PM$_{2.5-0.94}$) for the (a) polluted, (b) transition, and (c) clean periods. Any parameter with percent mass composition ≤ 5% is grouped into the 'other' category of each diagram. Mean mass concentrations associated with PM$_{0.94}$ and PM$_{2.5-0.94}$ for the three time periods (weighted by sample duration for each period) are provided next to each pie.

6.4 Nitrate-dominated Haze Event

Contrasting this pollution event with another one investigated during KORUS-AQ (May – June 2016) points to a difference in the relative amount of NO_3^- versus SO_4^{2-} (Jordan et al., 2020). The KORUS-AQ event exhibited comparable amounts between the two species. Compared to that event's concentrations, NO_3^- is about an order of magnitude larger in this study, while SO_4^{2-} is only about a factor of two greater. Gas-phase SO_2 is comparable between the two events. The difference is most likely explained by the much lower temperatures in the March 2019 event relative to the other study, which is thermodynamically more favorable for HNO_3

partitioning to the particle phase to increase NO_3^- levels (Seinfeld and Pandis, 2016). The ratio NO_3^-:SO_4^{2-} based on the full size distribution of the Inha filter sets was ~2.1 during the polluted period, where for the Seoul $PM_{2.5}$ data the ratio was ~2.2. The relative production of NO_3^- relative to SO_4^{2-} likely varies seasonally with colder temperatures and higher humidity more conducive to higher NO_3^- and thus $PM_{2.5}$ levels. High NO_3^- events were not particularly common, as shown especially for Beijing (Yang et al., 2017), requiring favorable conditions such as cold temperatures, high humidity, a shallow boundary layer, and high precursor levels. However, with reductions in sulfate precursor emissions, high NO_3^- events are increasingly reported in the literature (e.g., Xu et al., 2019; Zhou et al., 2022). The factors observed here in the March 2019 transboundary pollution event led to high NO_3^- levels.

7 Conclusions

This work relies on a unique dataset collected during a major transboundary pollution event that impacted the Korean peninsula in March 2019. In-situ gas, aerosol, and meteorological data are compared between Incheon (coastal) and Seoul (inland) along with the use of HYSPLIT and NAAPS reanalysis data. The results reveal notable features that are important for both regulatory purposes and general understanding of aerosol transport and formation processes.

- The pollution event stemmed from westerly transport under meteorological conditions that promoted secondary inorganic aerosol production in Incheon and Seoul.
- Seoul exhibited significantly higher $PM_{2.5}$ levels than Incheon during the polluted period with the difference arising from some combination of local emissions and extensive secondary aerosol formation due to favorable environmental conditions: low temperatures, elevated q and RH, and a shallow boundary layer.
- Secondarily produced inorganic and organic acids exhibited significant mass concentrations above 0.94 µm during the polluted period (~40% of total mass), and their size-resolved concentrations were highly correlated ($0.94 \leq r \leq 1.00$). The lack of coarse particle influence in promoting concentrations of species like SO_4^{2-}, NO_3^-, NH_4^+, and oxalate provided added support for the role of secondary aerosol formation assisted by high humidity. $PM_{2.5}$ at Seoul and Incheon were best related to q and RH as compared to other examined meteorological parameters. The higher humidities during the polluted period were coincident with increased sulfur and nitrogen oxidation ratios. This highlights the importance of heterogeneous processing and hygroscopic growth in contributing to the high supermicrometer concentrations of inorganic and organic acids in the polluted period. Increased particle size with hygroscopic growth in the humid conditions likely led to increased chemical uptake.
- High values of both NO_3^- mass and NO_3^-:SO_4^{2-} mass ratios were observed at both Incheon and Seoul, likely due to low temperatures promoting efficient NO_3^- formation.

The size distribution information from this work addresses specific concerns that have been raised about the applicability of PM_1 composition datasets to understanding $PM_{2.5}$ air quality exceedances in East Asian haze events. Here, we show that $PM_{2.5}$ composition apportionment for water-soluble ions is fully captured by the PM_1 fraction for this haze pollution event. Greater differences in the composition apportionment were observed for other atmospheric conditions after the haze period of this study. The contrast in the dominance of NO_3^- here (March 2019, T ≈ 9°C) versus the comparable amounts of NO_3^- and SO_4^{2-} observed during the KORUS-AQ campaign haze event (May 2016, T ≈ 20°C) points to the importance of conducting measurements at different times of the year to more fully understand haze formation and its impacts on air quality. Equally important is the use of these data to rigorously test apportionment of $PM_{2.5}$ composition in air quality models to ensure that the integrated impacts of transport and enhanced chemistry are adequately represented. This work contributes to the growing body of data required for ongoing model assessments of $PM_{2.5}$ that will inform mitigation strategies to improve air quality in South Korea.

Data Availability.
The sampled aerosol and meteorological data used in this study can be accessed at https://doi.org/10.6084/m9.figshare.16910686.v1. The NAAPS data used in this study can be accessed at https://nrlgodae1.nrlmry.navy.mil/cgi-bin/datalist.pl?dset=nrl_naaps_reanalysis&summary=Go.

Author contributions.

591 Joseph Schlosser, Armin Sorooshian, Carolyn Jordan, Katharine Travis, and James Crawford performed the
592 analysis and prepared the manuscript. Jong-sang Youn, Connor Stahl, and Yen Thi-Hoang Le, Hye-Jung Shin,
593 and In-ho Song conducted sample collection and/or analysis. All authors provided editorial support.
594

595 *Competing interests.*
596 The authors declare that they have no conflict of interest.
597

598 *Acknowledgements.*
599 Incheon (Inha University) data were provided by the Particle Pollution Research and Management Center. Seoul
600 monitoring data were provided by the National Institute of Environmental Research (NIER, NIER-2021-03-03-
601 001). We acknowledge the use of imagery from the NASA Worldview application
602 (https://worldview.earthdata.nasa.gov), part of the NASA Earth Observing System Data and Information System
603 (EOSDIS). The authors acknowledge the NOAA Air Resources Laboratory (ARL) for the provision of the
604 HYSPLIT transport and dispersion model and READY website (http://ready.arl.noaa.gov, last access: 27 October
605 2021) used in this work.

606

607 *Financial Support.*
608 This research was supported by the FRIEND (Fine Particle Research Initiative in East Asia Considering National
609 Differences) Project through the National Research Foundation of Korea (NRF) funded by the Ministry of Science
610 and ICT. (2020M3G1A1114626). Data analysis was funded by ONR grants N00014-21-1-2115 and
611 N0001421WX00227. In addition, this work was supported by the Catholic University of Korea, Research Fund,
612 2021.

613

References

Aldhaif, A. M., Lopez, D. H., Dadashazar, H., Painemal, D., Peters, A. J., and Sorooshian, A.: An Aerosol Climatology and Implications for Clouds at a Remote Marine Site: Case Study Over Bermuda, J. Geophys. Res. Atmos., 126, e2020JD034038, https://doi.org/10.1029/2020JD034038, 2021.

Arimoto, R., Duce, R. A., Savoie, D. L., and Prospero, J. M.: Trace elements in aerosol particles from Bermuda and Barbados: Concentrations, sources and relationships to aerosol sulfate, J. Atmos. Chem., 14, 439-457, 10.1007/BF00115250, 1992.

AzadiAghdam, M., Braun, R. A., Edwards, E.-L., Bañaga, P. A., Cruz, M. T., Betito, G., Cambaliza, M. O., Dadashazar, H., Lorenzo, G. R., Ma, L., MacDonald, A. B., Nguyen, P., Simpas, J. B., Stahl, C., and Sorooshian, A.: On the nature of sea salt aerosol at a coastal megacity: Insights from Manila, Philippines in Southeast Asia, Atmos. Environ., 216, 116922, https://doi.org/10.1016/j.atmosenv.2019.116922, 2019.

Bolton, D.: The Computation of Equivalent Potential Temperature, Monthly Weather Review, 108, 1046-1053, 10.1175/1520-0493(1980)108<1046:tcoept>2.0.co;2, 1980.

Cha, Y., Lee, S., and Lee, J.: Measurement of Black Carbon Concentration and Comparison with PM10 and PM2.5 Concentrations Monitored in Chungcheong Province, Korea, Aerosol Air Qual. Res., 19, 541-547, 10.4209/aaqr.2018.08.0325, 2019.

Chen, Y., Wild, O., Wang, Y., Ran, L., Teich, M., Größ, J., Wang, L., Spindler, G., Herrmann, H., van Pinxteren, D., McFiggans, G., and Wiedensohler, A.: The influence of impactor size cut-off shift caused by hygroscopic growth on particulate matter loading and composition measurements, Atmospheric Environment, 195, 141-148, https://doi.org/10.1016/j.atmosenv.2018.09.049, 2018.

Cheng, Y., Zheng, G., Wei, C., Mu, Q., Zheng, B., Wang, Z., Gao, M., Zhang, Q., He, K., Carmichael, G., Pöschl, U., and Su, H.: Reactive nitrogen chemistry in aerosol water as a source of sulfate during haze events in China, Sci. Adv., 2, e1601530, 10.1126/sciadv.1601530, 2016.

Cho, J. H., Kim, H. S., and Chung, Y. S.: Spatio-temporal changes of PM10 trends in South Korea caused by East Asian atmospheric variability, Air Qual. Atmos. Health, 14, 1001-1016, 10.1007/s11869-021-00995-y, 2021.

Choi, J., Park, R. J., Lee, H.-M., Lee, S., Jo, D. S., Jeong, J. I., Henze, D. K., Woo, J.-H., Ban, S.-J., Lee, M.-D., Lim, C.-S., Park, M.-K., Shin, H. J., Cho, S., Peterson, D., and Song, C.-K.: Impacts of local vs. trans-boundary emissions from different sectors on PM2.5 exposure in South Korea during the KORUS-AQ campaign, Atmos. Environ., 203, 196-205, https://doi.org/10.1016/j.atmosenv.2019.02.008, 2019a.

Choi, M., Lim, H., Kim, J., Lee, S., Eck, T. F., Holben, B. N., Garay, M. J., Hyer, E. J., Saide, P. E., and Liu, H.: Validation, comparison, and integration of GOCI, AHI, MODIS, MISR, and VIIRS aerosol optical depth over East Asia during the 2016 KORUS-AQ campaign, Atmos. Meas. Tech., 12, 4619-4641, 10.5194/amt-12-4619-2019, 2019b.

Colbeck, I., and Harrison, R. M.: Ozone—secondary aerosol—visibility relationships in North-West England, Sci. Total Environ., 34, 87-100, 1984.

Crosbie, E., Sorooshian, A., Monfared, N. A., Shingler, T., and Esmaili, O.: A Multi-Year Aerosol Characterization for the Greater Tehran Area Using Satellite, Surface, and Modeling Data, Atmosphere, 5, 178-197, 2014.

Cruz, M. T., Bañaga, P. A., Betito, G., Braun, R. A., Stahl, C., Aghdam, M. A., Cambaliza, M. O., Dadashazar, H., Hilario, M. R., Lorenzo, G. R., Ma, L., MacDonald, A. B., Pabroa, P. C., Yee, J. R., Simpas, J. B., and Sorooshian, A.: Size-resolved composition and morphology of particulate matter during the southwest monsoon in Metro Manila, Philippines, Atmos. Chem. Phys., 19, 10675-10696, 10.5194/acp-19-10675-2019, 2019.

Dadashazar, H., Alipanah, M., Hilario, M. R. A., Crosbie, E., Kirschler, S., Liu, H., Moore, R. H., Peters, A. J., Scarino, A. J., Shook, M., Thornhill, K. L., Voigt, C., Wang, H., Winstead, E., Zhang, B., Ziemba, L., and Sorooshian, A.: Aerosol Responses to Precipitation Along North American Air Trajectories Arriving at Bermuda, Atmos. Chem. Phys. Discuss., 2021, 1-34, 10.5194/acp-2021-471, 2021.

Eck, T. F., Holben, B. N., Kim, J., Beyersdorf, A. J., Choi, M., Lee, S., Koo, J. H., Giles, D. M., Schafer, J. S., Sinyuk, A., Peterson, D. A., Reid, J. S., Arola, A., Slutsker, I., Smirnov, A., Sorokin, M., Kraft, J., Crawford, J. H., Anderson, B. E., Thornhill, K. L., Diskin, G., Kim, S.-W., and Park, S.: Influence of cloud, fog, and high relative humidity during pollution transport events in South Korea: Aerosol properties and PM2.5 variability, Atmos. Environ., 232, 117530, https://doi.org/10.1016/j.atmosenv.2020.117530, 2020.

Ervens, B., Feingold, G., Frost, G. J., and Kreidenweis, S. M.: A modeling study of aqueous production of dicarboxylic acids: 1. Chemical pathways and speciated organic mass production, J. Geophys. Res. Atmos., 109, https://doi.org/10.1029/2003JD004387, 2004.

Fishman, J., and Seiler, W.: Correlative nature of ozone and carbon monoxide in the troposphere: Implications for the tropospheric ozone budget, J. Geophys. Res. Oceans, 88, 3662-3670, https://doi.org/10.1029/JC088iC06p03662, 1983.

Gelaro, R., McCarty, W., Suárez, M. J., Todling, R., Molod, A., Takacs, L., Randles, C., Darmenov, A., Bosilovich, M. G., Reichle, R., Wargan, K., Coy, L., Cullather, R., Draper, C., Akella, S., Buchard, V., Conaty, A., da Silva, A., Gu, W., Kim, G.-K., Koster, R., Lucchesi, R., Merkova, D., Nielsen, J. E., Partyka, G., Pawson, S., Putman, W., Rienecker, M., Schubert, S. D., Sienkiewicz, M., and Zhao, B.: The Modern-Era Retrospective Analysis for Research and Applications, Version 2 (MERRA-2), J. Clim., Volume 30, 5419-5454, 10.1175/JCLI-D-16-0758.1, 2017.

GMAO: MERRA-2 tavg1_2d_flx_Nx: 2d,1-Hourly,Time-Averaged,Single-Level,Assimilation,Surface Flux Diagnostics V5.12.4, in, edited by: DISC), G. E. S. D. a. I. S. C. G., Greenbelt, MD, 2015.

Guttikunda, S. K., Carmichael, G. R., Calori, G., Eck, C., and Woo, J.-H.: The contribution of megacities to regional sulfur pollution in Asia, Atmos. Environ., 37, 11-22, https://doi.org/10.1016/S1352-2310(02)00821-X, 2003.

Halliday, H. S., DiGangi, J. P., Choi, Y., Diskin, G. S., Pusede, S. E., Rana, M., Nowak, J. B., Knote, C., Ren, X., He, H., Dickerson, R. R., and Li, Z.: Using Short-Term CO/CO2 Ratios to Assess Air Mass Differences Over the Korean Peninsula During KORUS-AQ, J. Geophys. Res. Atmos., 124, 10951-10972, https://doi.org/10.1029/2018JD029697, 2019.

Heim, E. W., Dibb, J., Scheuer, E., Jost, P. C., Nault, B. A., Jimenez, J. L., Peterson, D., Knote, C., Fenn, M., Hair, J., Beyersdorf, A. J., Corr, C., and Anderson, B. E.: Asian dust observed during KORUS-AQ facilitates the uptake and incorporation of soluble pollutants during transport to South Korea, Atmos. Environ., 224, 117305, https://doi.org/10.1016/j.atmosenv.2020.117305, 2020.

Hennigan, C. J., Bergin, M. H., Dibb, J. E., and Weber, R. J.: Enhanced secondary organic aerosol formation due to water uptake by fine particles, Geophys. Res. Lett., 35, https://doi.org/10.1029/2008GL035046, 2008.

Hennigan, C. J., Bergin, M. H., Russell, A. G., Nenes, A., and Weber, R. J.: Gas/particle partitioning of water-soluble organic aerosol in Atlanta, Atmos. Chem. Phys., 9, 3613-3628, 10.5194/acp-9-3613-2009, 2009.

Hersey, S. P., Garland, R. M., Crosbie, E., Shingler, T., Sorooshian, A., Piketh, S., and Burger, R.: An overview of regional and local characteristics of aerosols in South Africa using satellite, ground, and modeling data, Atmos. Chem. Phys., 15, 4259-4278, 10.5194/acp-15-4259-2015, 2015.

Hilario, M. R. A., Crosbie, E., Bañaga, P. A., Betito, G., Braun, R. A., Cambaliza, M. O., Corral, A. F., Cruz, M. T., Dibb, J. E., Lorenzo, G. R., MacDonald, A. B., Robinson, C. E., Shook, M. A., Simpas, J. B., Stahl, C., Winstead, E., Ziemba, L. D., and Sorooshian, A.: Particulate Oxalate-To-Sulfate Ratio as an Aqueous Processing Marker: Similarity Across Field Campaigns and Limitations, Geophys. Res. Lett., 48, e2021GL096520, https://doi.org/10.1029/2021GL096520, 2021a.

Hilario, M. R. A., Crosbie, E., Shook, M., Reid, J. S., Cambaliza, M. O. L., Simpas, J. B. B., Ziemba, L., DiGangi, J. P., Diskin, G. S., Nguyen, P., Turk, F. J., Winstead, E., Robinson, C. E., Wang, J., Zhang, J., Wang, Y., Yoon, S., Flynn, J., Alvarez, S. L., Behrangi, A., and Sorooshian, A.: Measurement report: Long-range transport patterns into the tropical northwest Pacific during the CAMP2Ex aircraft campaign: chemical composition, size distributions, and the impact of convection, Atmos. Chem. Phys., 21, 3777-3802, 10.5194/acp-21-3777-2021, 2021b.

Hogan, T. F., Liu, M., Ridout, J. A., Peng, M. S., Whitcomb, T. R., Ruston, B. C., Reynolds, C. A., Eckermann, S. D., Moskaitis, J. R., Baker, N. L., McCormack, J. P., Viner, K. C., McLay, J. G., Flatau, M. K., Xu, L., Chen, C., and Chang, S. W.: The Navy Global Environmental Model, Oceanography, 27, 116-125, 2014.

Hu, J., Wang, Y., Ying, Q., and Zhang, H.: Spatial and temporal variability of PM2.5 and PM10 over the North China Plain and the Yangtze River Delta, China, Atmos. Environ., 95, 598-609, https://doi.org/10.1016/j.atmosenv.2014.07.019, 2014.

Huang, R.-J., Zhang, Y., Bozzetti, C., Ho, K.-F., Cao, J.-J., Han, Y., Daellenbach, K. R., Slowik, J. G., Platt, S. M., Canonaco, F., Zotter, P., Wolf, R., Pieber, S. M., Bruns, E. A., Crippa, M., Ciarelli, G., Piazzalunga, A., Schwikowski, M., Abbaszade, G., Schnelle-Kreis, J., Zimmermann, R., An, Z., Szidat, S., Baltensperger, U., Haddad, I. E., and Prévôt, A. S. H.: High secondary aerosol contribution to particulate pollution during haze events in China, Nature, 514, 218-222, 10.1038/nature13774, 2014.

Huang, R. J., He, Y., Duan, J., Li, Y., Chen, Q., Zheng, Y., Chen, Y., Hu, W., Lin, C., Ni, H., Dai, W., Cao, J., Wu, Y., Zhang, R., Xu, W., Ovadnevaite, J., Ceburnis, D., Hoffmann, T., and O'Dowd, C. D.: Contrasting sources and processes of particulate species in haze days with low and high relative humidity in wintertime Beijing, Atmos. Chem. Phys., 20, 9101-9114, 10.5194/acp-20-9101-2020, 2020.

Hyer, E. J., Reid, J. S., and Zhang, J.: An over-land aerosol optical depth data set for data assimilation by filtering, correction, and aggregation of MODIS Collection 5 optical depth retrievals, Atmos. Meas. Tech., 4, 379-408, 10.5194/amt-4-379-2011, 2011.

Jeon, W., Park, J., Choi, Y., Mun, J., Kim, D., Kim, C.-H., Lee, H.-J., Bak, J., and Jo, H.-Y.: The mechanism of the formation of high sulfate concentrations over the Yellow Sea during the KORUS-AQ period: The effect of

transport/atmospheric chemistry and ocean emissions, Atmos. Res., 105756, https://doi.org/10.1016/j.atmosres.2021.105756, 2021.

Ji, Y., Qin, X., Wang, B., Xu, J., Shen, J., Chen, J., Huang, K., Deng, C., Yan, R., Xu, K., and Zhang, T.: Counteractive effects of regional transport and emission control on the formation of fine particles: a case study during the Hangzhou G20 summit, Atmos. Chem. Phys., 18, 13581-13600, 10.5194/acp-18-13581-2018, 2018.

Jordan, C. E., Crawford, J. H., Beyersdorf, A. J., Eck, T. F., Halliday, H. S., Nault, B. A., Chang, L.-S., Park, J., Park, R., Lee, G., Kim, H., Ahn, J.-y., Cho, S., Shin, H. J., Lee, J. H., Jung, J., Kim, D.-S., Lee, M., Lee, T., Whitehill, A., Szykman, J., Schueneman, M. K., Campuzano-Jost, P., Jimenez, J. L., DiGangi, J. P., Diskin, G. S., Anderson, B. E., Moore, R. H., Ziemba, L. D., Fenn, M. A., Hair, J. W., Kuehn, R. E., Holz, R. E., Chen, G., Travis, K., Shook, M., Peterson, D. A., Lamb, K. D., and Schwarz, J. P.: Investigation of factors controlling PM2.5 variability across the South Korean Peninsula during KORUS-AQ, Elementa, 8, 10.1525/elementa.424, 2020.

Kaneyasu, N., Ohta, S., and Murao, N.: Seasonal variation in the chemical composition of atmospheric aerosols and gaseous species in Sapporo, Japan, Atmos. Environ., 29, 1559-1568, https://doi.org/10.1016/1352-2310(94)00356-P, 1995.

Kim, H.-S., Chung, Y.-S., and Lee, S.-G.: Characteristics of aerosol types during large-scale transport of air pollution over the Yellow Sea region and at Cheongwon, Korea, in 2008, Environ. Monit. Assess., 184, 1973-1984, 10.1007/s10661-011-2092-9, 2012.

Kim, Y. P., and Lee, G.: Trend of Air Quality in Seoul: Policy and Science, Aerosol Air Qual. Res., 18, 2141-2156, 10.4209/aaqr.2018.03.0081, 2018.

Koo, J.-H., Kim, J., Lee, Y. G., Park, S. S., Lee, S., Chong, H., Cho, Y., Kim, J., Choi, K., and Lee, T.: The implication of the air quality pattern in South Korea after the COVID-19 outbreak, Sci. Rep., 10, 22462, 10.1038/s41598-020-80429-4, 2020.

Koo, Y.-S., Yun, H.-Y., Choi, D.-R., Han, J.-S., Lee, J.-B., and Lim, Y.-J.: An analysis of chemical and meteorological characteristics of haze events in the Seoul metropolitan area during January 12–18, 2013, Atmos. Environ., 178, 87-100, https://doi.org/10.1016/j.atmosenv.2018.01.037, 2018.

Population Statistics: https://kosis.kr/statHtml/statHtml.do?orgId=101&tblId=DT_1B040A3, 2021.

Lamb, K. D., Perring, A. E., Samset, B., Peterson, D., Davis, S., Anderson, B. E., Beyersdorf, A., Blake, D. R., Campuzano-Jost, P., Corr, C. A., Diskin, G. S., Kondo, Y., Moteki, N., Nault, B. A., Oh, J., Park, M., Pusede, S. E., Simpson, I. J., Thornhill, K. L., Wisthaler, A., and Schwarz, J. P.: Estimating Source Region Influences on Black Carbon Abundance, Microphysics, and Radiative Effect Observed Over South Korea, J. Geophys. Res. Atmos., 123, 13,527-513,548, https://doi.org/10.1029/2018JD029257, 2018.

Lee, D., Choi, J.-Y., Myoung, J., Kim, O., Park, J., Shin, H.-J., Ban, S.-J., Park, H.-J., and Nam, K.-P.: Analysis of a Severe PM2.5 Episode in the Seoul Metropolitan Area in South Korea from 27 February to 7 March 2019: Focused on Estimation of Domestic and Foreign Contribution, Atmosphere, 10, 756, 2019a.

Lee, J. Y., and Kim, Y. P.: Source apportionment of the particulate PAHs at Seoul, Korea: impact of long range transport to a megacity, Atmos. Chem. Phys., 7, 3587-3596, 10.5194/acp-7-3587-2007, 2007.

Lee, S., Hong, J., Cho, Y., Choi, M., Kim, J., Park, S. S., Ahn, J.-Y., Kim, S.-K., Moon, K.-J., Eck, T. F., Holben, B. N., and Koo, J.-H.: Characteristics of Classified Aerosol Types in South Korea during the MAPS-Seoul Campaign, Aerosol Air Qual. Res., 18, 2195-2206, 10.4209/aaqr.2017.11.0474, 2018.

Lee, S., Kim, J., Choi, M., Hong, J., Lim, H., Eck, T. F., Holben, B. N., Ahn, J.-Y., Kim, J., and Koo, J.-H.: Analysis of long-range transboundary transport (LRTT) effect on Korean aerosol pollution during the KORUS-AQ campaign, Atmos. Environ., 204, 53-67, https://doi.org/10.1016/j.atmosenv.2019.02.020, 2019b.

Lee, S., Kim, M., Kim, S.-Y., Lee, D.-W., Lee, H., Kim, J., Le, S., and Liu, Y.: Assessment of long-range transboundary aerosols in Seoul, South Korea from Geostationary Ocean Color Imager (GOCI) and ground-based observations, Environ. Pollut., 269, 115924, https://doi.org/10.1016/j.envpol.2020.115924, 2021.

Lee, Y.-N., Weber, R., Ma, Y., Orsini, D., Maxwell-Meier, K., Blake, D., Meinardi, S., Sachse, G., Harward, C., Chen, T.-Y., Thornton, D., Tu, F.-H., and Bandy, A.: Airborne measurement of inorganic ionic components of fine aerosol particles using the particle-into-liquid sampler coupled to ion chromatography technique during ACE-Asia and TRACE-P, J. Geophys. Res. Atmos., 108, https://doi.org/10.1029/2002JD003265, 2003.

Lennartson, E. M., Wang, J., Gu, J., Castro Garcia, L., Ge, C., Gao, M., Choi, M., Saide, P. E., Carmichael, G. R., Kim, J., and Janz, S. J.: Diurnal variation of aerosol optical depth and PM2.5 in South Korea: a synthesis from AERONET, satellite (GOCI), KORUS-AQ observation, and the WRF-Chem model, Atmos. Chem. Phys., 18, 15125-15144, 10.5194/acp-18-15125-2018, 2018.

Li, J., Zhang, Y.-L., Cao, F., Zhang, W., Fan, M., Lee, X., and Michalski, G.: Stable Sulfur Isotopes Revealed a Major Role of Transition-Metal Ion-Catalyzed SO2 Oxidation in Haze Episodes, Environ. Sci. Technol., 54, 2626-2634, 10.1021/acs.est.9b07150, 2020.

Li, K., Chen, L., White, S. J., Zheng, X., Lv, B., Lin, C., Bao, Z., Wu, X., Gao, X., Ying, F., Shen, J., Azzi, M., and Cen, K.: Chemical characteristics and sources of PM1 during the 2016 summer in Hangzhou, Environ. Pollut., 232, 42-54, https://doi.org/10.1016/j.envpol.2017.09.016, 2018.

Lynch, P., Reid, J. S., Westphal, D. L., Zhang, J., Hogan, T. F., Hyer, E. J., Curtis, C. A., Hegg, D. A., Shi, Y., Campbell, J. R., Rubin, J. I., Sessions, W. R., Turk, F. J., and Walker, A. L.: An 11-year global gridded aerosol optical thickness reanalysis (v1.0) for atmospheric and climate sciences, Geosci. Model Dev., 9, 1489-1522, 10.5194/gmd-9-1489-2016, 2016.

MacDonald, A. B., Dadashazar, H., Chuang, P. Y., Crosbie, E., Wang, H., Wang, Z., Jonsson, H. H., Flagan, R. C., Seinfeld, J. H., and Sorooshian, A.: Characteristic Vertical Profiles of Cloud Water Composition in Marine Stratocumulus Clouds and Relationships With Precipitation, J. Geophys. Res. Atmos., 123, 3704-3723, https://doi.org/10.1002/2017JD027900, 2018.

Maudlin, L. C., Wang, Z., Jonsson, H. H., and Sorooshian, A.: Impact of wildfires on size-resolved aerosol composition at a coastal California site, Atmos. Environ., 119, 59-68, https://doi.org/10.1016/j.atmosenv.2015.08.039, 2015.

Mora, M., Braun, R. A., Shingler, T., and Sorooshian, A.: Analysis of remotely sensed and surface data of aerosols and meteorology for the Mexico Megalopolis Area between 2003 and 2015, J. Geophys. Res. Atmos., 122, 8705-8723, https://doi.org/10.1002/2017JD026739, 2017.

Nault, B. A., Campuzano-Jost, P., Day, D. A., Schroder, J. C., Anderson, B., Beyersdorf, A. J., Blake, D. R., Brune, W. H., Choi, Y., Corr, C. A., de Gouw, J. A., Dibb, J., DiGangi, J. P., Diskin, G. S., Fried, A., Huey, L. G., Kim, M. J., Knote, C. J., Lamb, K. D., Lee, T., Park, T., Pusede, S. E., Scheuer, E., Thornhill, K. L., Woo, J. H., and Jimenez, J. L.: Secondary organic aerosol production from local emissions dominates the organic aerosol budget over Seoul, South Korea, during KORUS-AQ, Atmos. Chem. Phys., 18, 17769-17800, 10.5194/acp-18-17769-2018, 2018.

Paciga, A. L., Riipinen, I., and Pandis, S. N.: Effect of Ammonia on the Volatility of Organic Diacids, Environ. Sci. Technol., 48, 13769-13775, 10.1021/es5037805, 2014.

Park, G., Kim, K., Park, T., Kang, S., Ban, J., Choi, S., Yu, D.-G., Lee, S., Lim, Y., Kim, S., Mun, S., Woo, J.-H., Jeon, C.-S., and Lee, T.: Primary and secondary aerosols in small passenger vehicle emissions: Evaluation of engine technology, driving conditions, and regulatory standards, Environ. Pollut., 286, 117195, https://doi.org/10.1016/j.envpol.2021.117195, 2021.

Park, I.-S., Park, M.-S., Jang, Y. W., Kim, H.-K., Song, C.-K., Owen, J. S., Kim, S.-H., Cho, C.-R., and Kim, C.-H.: Impact Comparison of Synoptic Meteorology and Nationwide/local Emissions on the Seoul Metropolitan Area during High PM Multi-event and Non-event Days, 10.5572/ajae.2020.14.3.263, 2020a.

Park, S.-M., Song, I.-H., Park, J. S., Oh, J., Moon, K. J., Shin, H. J., Ahn, J. Y., Lee, M.-D., Kim, J., and Lee, G.: Variation of PM2.5 Chemical Compositions and their Contributions to Light Extinction in Seoul, Aerosol Air Qual. Res., 18, 2220-2229, 10.4209/aaqr.2017.10.0369, 2018.

Park, S., Thi Hong, H. D., Cho, S. Y., and Bae, M.-S.: Chemical Composition and Light Absorption of PM2.5 Observed at Two Sites near a Busy Road during Summer and Winter, Appl. Sci., 10, 4858, 2020b.

Peterson, D. A., Hyer, E. J., Han, S.-O., Crawford, J. H., Park, R. J., Holz, R., Kuehn, R. E., Eloranta, E., Knote, C., Jordan, C. E., and Lefer, B. L.: Meteorology influencing springtime air quality, pollution transport, and visibility in Korea, Elementa, 7, 10.1525/elementa.395, 2019.

Quan, J., Liu, Q., Li, X., Gao, Y., Jia, X., Sheng, J., and Liu, Y.: Effect of heterogeneous aqueous reactions on the secondary formation of inorganic aerosols during haze events, Atmos. Environ., 122, 306-312, https://doi.org/10.1016/j.atmosenv.2015.09.068, 2015.

Rolph, G., Stein, A., and Stunder, B.: Real-time Environmental Applications and Display sYstem: READY, Environ. Model Softw., 95, 210-228, https://doi.org/10.1016/j.envsoft.2017.06.025, 2017.

Ryu, Y.-H., and Min, S.-K.: Long-term evaluation of atmospheric composition reanalyses from CAMS, TCR-2, and MERRA-2 over South Korea: Insights into applications, implications, and limitations, Atmos. Environ., 246, 118062, https://doi.org/10.1016/j.atmosenv.2020.118062, 2021.

Ryu, Y.-H., Min, S.-K., and Hodzic, A.: Recent Decreasing Trends in Surface PM2.5 over East Asia in the Winter-spring Season: Different Responses to Emissions and Meteorology between Upwind and Downwind Regions, Aerosol Air Qual. Res., 21, 200654, 10.4209/aaqr.200654, 2021.

Seinfeld, J. H., and Pandis, S. N.: Atmospheric Chemistry and Physics, 3 ed., Wiley-Interscience, New York, 2016.

Seo, J., Park, D. S. R., Kim, J. Y., Youn, D., Lim, Y. B., and Kim, Y.: Effects of meteorology and emissions on urban air quality: a quantitative statistical approach to long-term records (1999–2016) in Seoul, South Korea, Atmos. Chem. Phys., 18, 16121-16137, 10.5194/acp-18-16121-2018, 2018.

Seo, J., Lim, Y. B., Youn, D., Kim, J. Y., and Jin, H. C.: Synergistic enhancement of urban haze by nitrate uptake into transported hygroscopic particles in the Asian continental outflow, Atmos. Chem. Phys., 20, 7575-7594, 10.5194/acp-20-7575-2020, 2020.

Shao, J., Chen, Q., Wang, Y., Lu, X., He, P., Sun, Y., Shah, V., Martin, R. V., Philip, S., Song, S., Zhao, Y., Xie, Z., Zhang, L., and Alexander, B.: Heterogeneous sulfate aerosol formation mechanisms during wintertime Chinese haze events: air quality model assessment using observations of sulfate oxygen isotopes in Beijing, Atmos. Chem. Phys., 19, 6107-6123, 10.5194/acp-19-6107-2019, 2019.

Sorooshian, A., Varutbangkul, V., Brechtel, F. J., Ervens, B., Feingold, G., Bahreini, R., Murphy, S. M., Holloway, J. S., Atlas, E. L., Buzorius, G., Jonsson, H., Flagan, R. C., and Seinfeld, J. H.: Oxalic acid in clear and cloudy atmospheres: Analysis of data from International Consortium for Atmospheric Research on Transport and Transformation 2004, J. Geophys. Res. Atmos., 111, https://doi.org/10.1029/2005JD006880, 2006.

Sorooshian, A., Lu, M.-L., Brechtel, F. J., Jonsson, H., Feingold, G., Flagan, R. C., and Seinfeld, J. H.: On the Source of Organic Acid Aerosol Layers above Clouds, Environ. Sci. Technol., 41, 4647-4654, 10.1021/es0630442, 2007.

Sorooshian, A., Murphy, S. M., Hersey, S., Bahreini, R., Jonsson, H., Flagan, R. C., and Seinfeld, J. H.: Constraining the contribution of organic acids and AMS m/z 44 to the organic aerosol budget: On the importance of meteorology, aerosol hygroscopicity, and region, Geophys. Res. Lett., 37, https://doi.org/10.1029/2010GL044951, 2010.

Stahl, C., Cruz, M. T., Bañaga, P. A., Betito, G., Braun, R. A., Aghdam, M. A., Cambaliza, M. O., Lorenzo, G. R., MacDonald, A. B., Pabroa, P. C., Yee, J. R., Simpas, J. B., and Sorooshian, A.: An annual time series of weekly size-resolved aerosol properties in the megacity of Metro Manila, Philippines, Sci. Data, 7, 128, 10.1038/s41597-020-0466-y, 2020.

Stein, A. F., Draxler, R. R., Rolph, G. D., Stunder, B. J. B., Cohen, M. D., and Ngan, F.: NOAA's hysplit atmospheric transport and dispersion modeling system, in: Bull. Am. Meteorol. Soc., 12, 2059+, 2015.

Wang, G., Zhang, R., Gomez, M. E., Yang, L., Levy Zamora, M., Hu, M., Lin, Y., Peng, J., Guo, S., Meng, J., Li, J., Cheng, C., Hu, T., Ren, Y., Wang, Y., Gao, J., Cao, J., An, Z., Zhou, W., Li, G., Wang, J., Tian, P., Marrero-Ortiz, W., Secrest, J., Du, Z., Zheng, J., Shang, D., Zeng, L., Shao, M., Wang, W., Huang, Y., Wang, Y., Zhu, Y., Li, Y., Hu, J., Pan, B., Cai, L., Cheng, Y., Ji, Y., Zhang, F., Rosenfeld, D., Liss, P. S., Duce, R. A., Kolb, C. E., and Molina, M. J.: Persistent sulfate formation from London Fog to Chinese haze, Proc. Natl. Acad. Sci. U.S.A., 113, 13630-13635, 10.1073/pnas.1616540113, 2016.

Wang, J., Li, J., Ye, J., Zhao, J., Wu, Y., Hu, J., Liu, D., Nie, D., Shen, F., Huang, X., Huang, D. D., Ji, D., Sun, X., Xu, W., Guo, J., Song, S., Qin, Y., Liu, P., Turner, J. R., Lee, H. C., Hwang, S., Liao, H., Martin, S. T., Zhang, Q., Chen, M., Sun, Y., Ge, X., and Jacob, D. J.: Fast sulfate formation from oxidation of SO2 by NO2 and HONO observed in Beijing haze, Nat. Commun., 11, 2844, 10.1038/s41467-020-16683-x, 2020.

Weinstock, B.: Carbon Monoxide: Residence Time in the Atmosphere, Science, 166, 224-225, doi:10.1126/science.166.3902.224, 1969.

Won, W.-S., Oh, R., Lee, W., Kim, K.-Y., Ku, S., Su, P.-C., and Yoon, Y.-J.: Impact of Fine Particulate Matter on Visibility at Incheon International Airport, South Korea, Aerosol Air Qual. Res., 1048-1061, 10.4209/aaqr.2019.03.0106, 2020.

Wonaschuetz, A., Sorooshian, A., Ervens, B., Chuang, P. Y., Feingold, G., Murphy, S. M., de Gouw, J., Warneke, C., and Jonsson, H. H.: Aerosol and gas re-distribution by shallow cumulus clouds: An investigation using airborne measurements, J. Geophys. Res. Atmos., 117, https://doi.org/10.1029/2012JD018089, 2012.

Wu, Y., Ge, X., Wang, J., Shen, Y., Ye, Z., Ge, S., Wu, Y., Yu, H., and Chen, M.: Responses of secondary aerosols to relative humidity and photochemical activities in an industrialized environment during late winter, Atmos. Environ., 193, 66-78, https://doi.org/10.1016/j.atmosenv.2018.09.008, 2018.

Xu, Q., Wang, S., Jiang, J., Bhattarai, N., Li, X., Chang, X., Qiu, X., Zheng, M., Hua, Y., and Hao, J.: Nitrate dominates the chemical composition of $PM_{2.5}$ during haze event in Beijing, China, Science of The Total Environment, 689, 1293-1303, https://doi.org/10.1016/j.scitotenv.2019.06.294, 2019.

Yang, T., Sun, Y., Zhang, W., Wang, Z., Liu, X., Fu, P., and Wang, X.: Evolutionary processes and sources of high-nitrate haze episodes over Beijing, Spring, J. Environ. Sci., 54, 142-151, https://doi.org/10.1016/j.jes.2016.04.024, 2017.

Yu, J. Z., Huang, X.-F., Xu, J., and Hu, M.: When Aerosol Sulfate Goes Up, So Does Oxalate: Implication for the Formation Mechanisms of Oxalate, Environ. Sci. Technol., 39, 128-133, 10.1021/es049559f, 2005.

Zhang, C., Lu, X., Zhai, J., Chen, H., Yang, X., Zhang, Q., Zhao, Q., Fu, Q., Sha, F., and Jin, J.: Insights into the formation of secondary organic carbon in the summertime in urban Shanghai, J. Environ. Sci., 72, 118-132, https://doi.org/10.1016/j.jes.2017.12.018, 2018.

Zhang, J., and Reid, J. S.: MODIS aerosol product analysis for data assimilation: Assessment of over-ocean level 2 aerosol optical thickness retrievals, J. Geophys. Res. Atmos., 111, https://doi.org/10.1029/2005JD006898, 2006.

Zhang, Q., Worsnop, D. R., Canagaratna, M. R., and Jimenez, J. L.: Hydrocarbon-like and oxygenated organic aerosols in Pittsburgh: insights into sources and processes of organic aerosols, Atmos. Chem. Phys., 5, 3289-3311, 10.5194/acp-5-3289-2005, 2005.

Zhang, R., Wang, G., Guo, S., Zamora, M. L., Ying, Q., Lin, Y., Wang, W., Hu, M., and Wang, Y.: Formation of Urban Fine Particulate Matter, Chemical Reviews, 115, 3803-3855, 10.1021/acs.chemrev.5b00067, 2015.

Zhang, T., Shen, Z. X., Su, H., Liu, S. X., Zhou, J. M., Zhao, Z. Z., Wang, Q. Y., Prévôt, A. S. H., and Cao, J. J.: Effects of Aerosol Water Content on the formation of secondary inorganic aerosol during a Winter Heavy PM2.5 Pollution Episode in Xi'an, China, Atmos. Environ., 252, 118304, https://doi.org/10.1016/j.atmosenv.2021.118304, 2021.

Zhang, Y., Tang, L., Croteau, P. L., Favez, O., Sun, Y., Canagaratna, M. R., Wang, Z., Couvidat, F., Albinet, A., Zhang, H., Sciare, J., Prévôt, A. S. H., Jayne, J. T., and Worsnop, D. R.: Field characterization of the PM2.5 Aerosol Chemical Speciation Monitor: insights into the composition, sources, and processes of fine particles in eastern China, Atmos. Chem. Phys., 17, 14501-14517, 10.5194/acp-17-14501-2017, 2017.

Zhou, Y., Huang, X. H., Bian, Q., Griffith, S. M., Louie, P. K. K., and Yu, J. Z.: Sources and atmospheric processes impacting oxalate at a suburban coastal site in Hong Kong: Insights inferred from 1 year hourly measurements, J. Geophys. Res. Atmos., 120, 9772-9788, https://doi.org/10.1002/2015JD023531, 2015.

Zhou, M., Nie, W., Qiao, L., Huang, D. D., Zhu, S., Lou, S., Wang, H., Wang, Q., Tao, S., Sun, P., Liu, Y., Xu, Z., An, J., Yan, R., Su, H., Huang, C., Ding, A., and Chen, C.: Elevated formation of particulate nitrate from N_2O_5 hydrolysis in the Yangtze River Delta region from 2011 to 2019, Geophysical Research Letters, e2021GL097393, https://doi.org/10.1029/2021GL097393, 2022.